ANL/CFCT-25/16

Comprehensive Evaluation of the Advanced Moderator Module (AMM)

Microreactor Program M3 Report

About Argonne National Laboratory

Argonne is a U.S. Department of Energy laboratory managed by UChicago Argonne, LLC under contract DE-AC02-06CH11357. The Laboratory's main facility is outside Chicago, at 9700 South Cass Avenue, Argonne, Illinois 60439. For information about Argonne and its pioneering science and technology programs, see www.anl.gov.

ANL/CFCT-25/16

Comprehensive Evaluation of the Advanced Moderator Module (AMM)

Microreactor Program M3 Report

Prepared by

Sumit Bhattacharya, Abdellatif M. Yacout

Chemical & Fuel Cycle Technologies Division, Argonne National Laboratory

Dean Walters, Greg Fletcher

Experimental Operations and Facilities, Argonne National Laboratory

Darrell Cheu, Adrien Terricabras, Michael Hahn, Erik P. Luther, Caitlin Kohnert, Holly Trellue

Los Alamos National Laboratory

Prepared for

U.S. Department of Energy
Microreactor Program

August 30, 2025

ABSTRACT

The U.S. nuclear sector is now focusing on advancing and deploying microreactors that blend efficiency, compactness, and safety. For thermal neutron microreactors designed for high-temperature operations, employing a metal hydride-based moderator presents a valuable opportunity to enhance neutron efficiency. Argonne National Laboratory (ANL) has pioneered an Advanced Moderator Module (AMM) featuring an innovative containment strategy. This design leverages the strengths of refractory metals, ceramic matrix composites (CMCs), and state-of-the-art coatings to create a robust hydrogen (H_2) permeation barrier capable of withstanding extreme temperatures. At the core of the AMM is a metal hydride, such as YH_{2-x}, encased within a flexible niobium (Nb) liner. This liner is coated with a specialized H_2 barrier layer, developed at Argonne, to effectively minimize H_2 leakage at high temperatures. Surrounding this assembly is a silicon carbide (SiC) CMC cladding that provides structural integrity, particularly during power fluctuations, while a diffusion barrier between the cladding and the liner prevents chemical reactions at elevated temperatures. This comprehensive design aims to minimize H_2 loss throughout the microreactor's operational life.

This report presents the first AMM prototypes manufactured at ANL and highlights their performance with a particular focus on the end-cap regions, where hydrogen permeation is most critical. Since end caps are attached at the final stage of assembly, they often require recoating to restore barrier function; thus, developing simplified, reliable coating solutions is essential to streamline fabrication and reduce costs while ensuring long-term hydrogen retention.

Along with the Nb liner surface coatings, end-cap coatings are systematically evaluated, ranging from 0.5 μm single-layer Al_2O_3 films to 3.2 μm (8-layer) Cr/ Al_2O_3 multilayers. Performance testing was performed at 750 °C, under both high vacuum (~5×10^{-6} mbar, Argonne) and argon (1 atm, 50 sccm flow), with one study at 800 °C at Los Alamos National Laboratory (LANL). The testing revealed that end cap surface area can contribute to hydrogen loss due to niobium's poor permeation resistance, coupled with the significant mass loss observed from the SiC composite shell degassing under vacuum. Note that contributions from degassing was confirmed through direct weighting of the tested YH pellet and thermal testing of the SiC composite shells. H/Y ratio measurements confirmed that thin or single-layer coatings permit significant leakage, whereas multilayer coatings ≥1.8 μm substantially mitigate the hydrogen loss. In particular, the most optimized, 3.2 μm (8-layer) design limited hydrogen loss to very low values after 300 hours which is equivalent to a loss of <3% after 8500 hr. (~ one year) at 750 °C. Thermal-mechanical modeling further showed that stresses are governed by thermal expansion mismatch (Al_2O_3 vs Nb) and cap pressure gradients, with vacuum conditions promoting tensile-driven cracking and Argon atmosphere (1 ATM) shifting stresses toward stabilizing compression. Radial stress analyses indicated that multilayers distribute stress more evenly, while thin single layers suffer from large stress swings and are prone to delamination.

Overall, these results establish end-cap coating design as a key performance-limiting factor in AMMs. Optimized multilayers not only reduce hydrogen permeation but also improve coating durability, thereby enabling simplified manufacturing, lower costs, and reliable long-term operation under reactor-relevant conditions.

ACKNOWLEDGEMENT

This work is supported by the Microreactor Program of the US Department of Energy's (DOE)'s Office of Nuclear Energy. The efforts involving Argonne National Laboratory were supported under Contract No. DE-AC02-06CH11357 between UChicago Argonne, LLC and the U.S. Department of Energy.

TABLE OF CONTENTS

LIST OF FIGURES

welded end-cap region. (c) Top-down cross-section through the cap showing uniform weld and liner integrity.

Figure 10: Schematic of end-cap coating strategies after welding. (a) After Nb cap welding is completed, (b) Single-layer design (0.5 μm Al_2O_3). (c) Intermediate multilayer architectures (1.2–1.8 μm) with only the weld groove region left uncoated, highlighting the recoating approach for restoring barrier continuity at the welded end caps.

Figure 11: Representative SiC CMC shell (left) and measured weight-loss kinetics during de-gassing at 750 °C (right). Data are shown for two shell lengths (67 mm and 36.5 mm), indicating higher de-gassing contributions for longer shells. These results provide baseline correction factors for isolating true hydrogen loss from YH_{2-x} pellets in AMM modules.

Figure 12: A detailed analysis of the coating layers on the inside and outside surfaces of niobium (Nb) tubes used for doing further thermal studies. (a) The tube is cut to reveal the internal and external coating cross-sections on the tube surfaces. (a') FIB cross section of the inner surface area marked with red box, showing the developed CrAl/Al2O3 multilayer and (a") FIB cross section of the outer surface area marked with yellow box, showing the developed CrAl/Al2O3 multilayer.

Figure 13. Photographs of tested AMM modules with 500 nm Al_2O_3–coated end caps prior to thermal testing: (a) Argon-tested module and (b) vacuum-tested module.

Figure 14. Measured H/Y ratio evolution for AMM modules with 500 nm Al_2O_3–coated Nb end caps tested at 750 °C. (a) Argon (1 atm, 50 sccm flow) and (b) vacuum (~5×10^{-6} mbar). Both cases show substantial hydrogen loss, with ~21% loss in vacuum and ~18% loss in Argon, confirming that single-layer coatings are insufficient for H_2 retention.

Figure 15. Optical appearance of YH_{2-x} pellets: (a) as-prepared pellet showing the characteristic blue color of YH_{2-x}, (b) pellet recovered from AMM tested under vacuum, exhibiting metallic gray/light-blue surface due to severe hydrogen loss, and (c) pellet recovered from AMM tested under argon, retaining a lighter blue shade indicative of partial hydrogen retention.

Figure 16. AMM module used for the two-step test with 1.2 μm ($2\times Al_2O_3$ + 2×Cr) end-cap coating. (a) As-prepared YH_{2-x} pellet. (b) Coated AMM shell and a fully sealed module prior to testing.

Figure 17: A detailed examination of the coating applied over the welded Nb cap, after it has gone through thermal cycling exposures to 800 °C for 5 times. (a) Top view of the coated and welded Nb cap, (b, c, d, & e) Showing a cross-sectional FIB-SEM view of the deposited multilayer coating, over the welded Nb cap surface. The FIB reveals a well-adhered uniform coating with no visible defects or separations in all four regions.

Figure 18. Hydrogen-loss trajectories for the same AMM module with the 1.2 μm multilayer on end caps, (a) Argon, 750 °C, 500 h at ANL: shallow, ~linear decline corresponding to ≈2 % H loss. (b) High vacuum, 800 °C, 500 h at LANL: steeper decline corresponding to ≈7 % H loss, attributed to tensile stress in vacuum plus Arrhenius increase in permeability and higher thermal-mismatch stresses at 800 °C.

Figure 19. Appearance of YH_{2-x} pellets before and after AMM exposure: (a) as-prepared pellet showing uniform blue coloration, and (b) pellet recovered after sequential thermal exposures (500 h in Ar at 750 °C and 500 h in vacuum at 800 °C), showing blue surface with localized spotted discoloration due to hydrogen depletion.

Figure 20. Post-test evaluation of AMM with single-layer Al_2O_3 (500 nm) cap coating after 500 h exposure under vacuum at 750 °C: (a) intact AMM, (b) sectioned view showing intact multilayer inner liner coating, (c) Nb cap region with localized discoloration, and (d) weld region showing no visible failure or coating degradation.

Figure 21. SEM & EDS evaluation of the Nb end cap from the AMM module tested under vacuum for 500 h. (a) Optical image of the Nb cap surface; (b, c) SEM micrographs of the pan-shaped valley regions, showing localized cracking and spallation of the 500 nm Al_2O_3 single-layer coating along the edge transition zones. (c′) layered EDS map showing combined Nb, Al, and O signals, (c″) Al Kα1 distribution, (c‴) O Kα1 distribution, and (c⁗) Nb Lα1 distribution. Clear Nb signal confirms coating loss and substrate exposure in fractured regions of the single-layer Al_2O_3 design.

Figure 22. Optical images of the AMM module with multilayer-coated Nb cap region (2 × 300 nm Al_2O_3 + 2 × 300 nm Cr). (a) Whole AMM module following thermal testing, (b) split AMM exposing intact inner surfaces, (c) Nb cap region showing slight discoloration, and (d) weld region highlighting surface features following exposure.

Figure 23. EDS mapping and elemental analysis of the Nb end cap region coated with two Al_2O_3 + two Cr layers. (a) Optical image of the coated end cap, (b) composite layered EDS map, (c) Al $K\alpha_1$ distribution, (d) Cr $L\alpha_{1,2}$ distribution, and (e) Nb $L\alpha_1$ distribution.

Figure 24. FIB cross-sectional analysis of the optimized multilayer coating on the Nb liner surface of the AMM module tested under vacuum at 800 °C for 500 h. (a) Optical image of the outer surface, (a′) FIB cross-section from the outer surface, (b) optical image of the inner surface, and (b′) FIB cross-section from the inner surface showing intact multilayer structure. The analysis confirms coating stability and indicates that hydrogen loss arises from Nb end-cap regions rather than the optimized multilayer-coated liner surface.

Figure 25. Optical micrographs of AMM Nb weld cap regions for single-layer (a) and multilayer (b) coated designs, alongside corresponding SEM images from regions 1–4 (a′, a″, b′, b″). All

examined regions confirm weld integrity remains intact even after extended high-temperature cycling.

Figure 26. Hoop stress distribution in a 500 nm Al_2O_3 single-layer coating at 750 °C under vacuum and argon environments, showing rim stress concentrations driving fracture and coating failure.

Figure 27. Hoop stress distribution in the Nb end-cap region coated with a 1.2 μm multilayer stack (2×Cr-300 nm + 2×Al_2O_3-300 nm) tested at 750 °C, showing stress concentration at the rim and correlation with observed coating failure.

Figure 28. Optical images of recovered AMM modules with 3.2 μm multilayer coatings tested at 750 °C for 300 hours: (a) under argon atmosphere, and (b) under vacuum. Both show stable surfaces without spallation or visible degradation, particularly at the Nb cap regions, confirming structural integrity without SiC shell support.

Figure 29. Measured hydrogen weight retention profiles for the 3.2 μm multilayer-coated AMM modules tested at 750 °C: (a) under argon atmosphere for 300 hours, and (b) under vacuum for 300 hours. Both conditions show negligible hydrogen loss, indicating excellent hermetic performance of the multilayer stack at the Nb cap regions.

Figure 30. SEM–EDS analysis of the **Nb cap weld edges with a 3.2 μm thick multilayer coating, from the AMM tested under argon atmosphere** showing intact multilayer coating with no cracks, spallation, or Nb exposure.

Figure 31. SEM–EDS analysis of the **Nb cap weld edges from the AMM with 3.2 μm coated end cap, tested under vacuum atmosphere** demonstrating continuous multilayer coverage and absence of Nb signals, validating the stress-relief effect of multilayer stacking.

Figure 32: Hoop stress distribution in a 500 nm Al_2O_3 single-layer coating at 750 °C under vacuum and argon environments, showing rim stress concentrations driving fracture and coating failure.

1. Introduction

The U.S. nuclear industry is focusing on the development of transportable microreactors for civilian and military applications, led by a consortium of private industries [1, 2] along with support from the DOE-NE [1], DOE-ARPA-E , and DoD [2]. Among the technologies being explored, very-high-temperature gas-cooled (VHTR) and heat-pipe cooled reactors are favoured for their high efficiency, safety, and suitability for microreactor applications. These reactors utilize a Brayton cycle for efficient power generation at high temperatures and feature inherent safety mechanisms [3]. A critical component in these high-temperature reactors is graphite, used to moderate neutrons due to its durability and low absorption cross-section [4]. However, graphite presents challenges, such as less efficient neutron slowing compared to hydrogen-based materials, leading to a high carbon-to-U-235 ratio requirement, and the need for substantial volumes of graphite, which impacts the compactness and transportability of micro-reactors. Additionally, safety concerns arise in scenarios where the reactor core could be flooded, potentially causing instability [5].

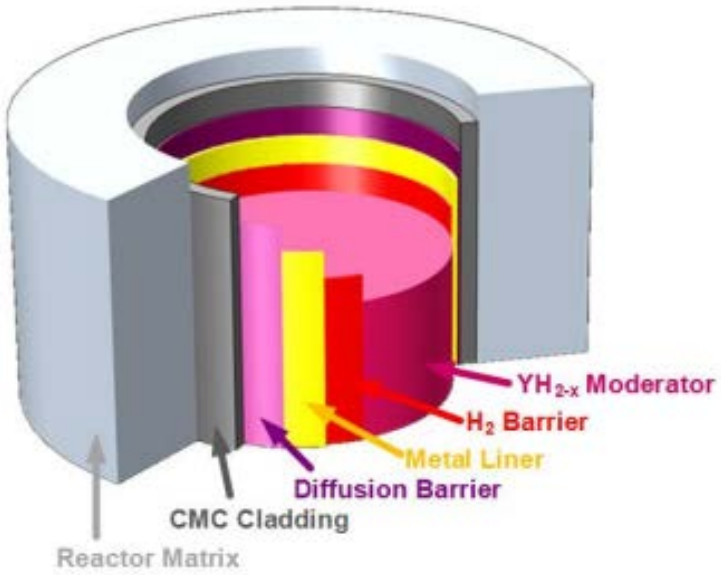

Figure 1: Schematic of the proposed Argonne AMM technology[5]

To address these challenges, there's a shift towards hydrogen-based alternatives [6], which offer better moderating efficiency and reduced weight. In response, Argonne National Laboratory

has developed an Advanced Moderator Module (AMM) that integrates refractory metals, ceramic matrix composites (CMCs), and advanced coatings to create an effective hydrogen permeation barrier, capable of withstanding extreme temperatures as shown in Figure 1.

The AMM features a metal hydride core, such as YH_2-x, encased in a ductile refractory niobium (Nb) liner, which is coated with an H_2 barrier layer developed at Argonne to minimize hydrogen leakage at high temperatures. This core is further protected by a silicon carbide (SiC) CMC cladding that provides structural support, particularly during power fluctuations, and includes a diffusion barrier between the cladding and liner to prevent chemical interactions at elevated temperatures. This design can effectively reduce hydrogen loss over the microreactor's operational life. The benefits of the AMM technology have been comprehensively assessed through a detailed multi-phase reactor physics analysis, with more information available in our previous report [5]. By utilizing advanced moderation techniques with metal hydrides like YH_2-x, the AMM enables optimal neutron moderation. Its encapsulation method outperforms traditional approaches, offering lower thermal neutron absorption rates compared to those using stainless steel or other high-temperature alloys. This results in improved neutron economy, a crucial factor for developing smaller microreactor cores with extended operational lifetimes.

Through this report, we are showcasing the first AMM modules that have been manufactured at Argonne National laboratory and emphasizing their performance, with a particular focus on the end-cap regions where hydrogen permeation has been found to be most critical. This study highlights the importance of coating architecture and design optimization for the end caps. The rationale is as the end caps are attached at the final stage of assembly, necessitating recoating to restore barrier function of the AMM encapsulating liner. A simplified, reliable coating solution for the end caps can therefore streamline the AMM manufacturing process, saving both time and cost, while ensuring that the hydrogen retention performance of the module is not compromised. Despite their relatively small surface area compared to the cylindrical liner, the end caps were shown to be major contributors to H_2 loss, owing to niobium's intrinsically high hydrogen permeability. As a result, the effectiveness of the applied coatings directly determines the hydrogen retention capacity of the AMM. Measured H/Y ratio evolution confirmed that thinner or single-layer coatings allow significant hydrogen leakage, while multilayer coatings $\geq$1.8 μm drastically reduce loss. Notably, the 3.2 μm (8-layer) coating limited hydrogen loss to <3% after 300 h, approaching performance targets for long-duration operation.

Thermal-mechanical modeling revealed that coating stresses are strongly influenced by both thermal expansion mismatch (Al_2O_3 vs Nb) and the local pressure gradient at the cap region. Radial and cross-sectional stress profiles demonstrated that multilayer architectures distribute stress more evenly, while single thin layers (e.g., 500 nm Al_2O_3) experience large compressive or tensile swings, making them prone to delamination.

Implications for AMM Design : The findings of this report establish that end-cap coating design is a primary performance-limiting factor in AMMs. Even small, exposed cap regions can dominate hydrogen loss if they are left poorly protected. Optimized multilayer coatings not only reduce permeation but also mitigate stress concentrations, thereby extending durability. By prioritizing end-cap coating strategies over complex weld modifications, this work demonstrates a pathway to; (a) Simplify AMM fabrication, (b) Lower production costs, and (c) Ensure long-term hydrogen retention under reactor-relevant conditions.

2. Materials and Methods:

2.1. Steps to manufacture a complete AMM part.

The AMM design incorporates a refractory liner that is coated on both its interior and exterior surfaces and is externally reinforced with a ceramic matrix composite (CMC) cladding, forming an effective containment system for the high-temperature hydride moderator. The interior surface of the liner is treated with a specialized hydrogen-impermeable layer, which effectively traps hydrogen, preventing both the embrittlement of the liner and the eventual escape of hydrogen that could occur due to migration into the liner material. Externally, the liner is protected by a diffusion barrier that reduces interactions between the CMC and the refractory metal. This barrier is critical for slowing the diffusion of silicon into the refractory metal liner, a process that could otherwise result in the formation of brittle intermetallic compounds, thus compromising the liner's resilience to thermal fluctuations, especially at elevated temperatures. Details about the coating and CMC cladding are provided in the subsequent section. To streamline the assembly process, manufacturing has been divided into three distinct stages, as illustrated in Figure 2 (a, b, and c).

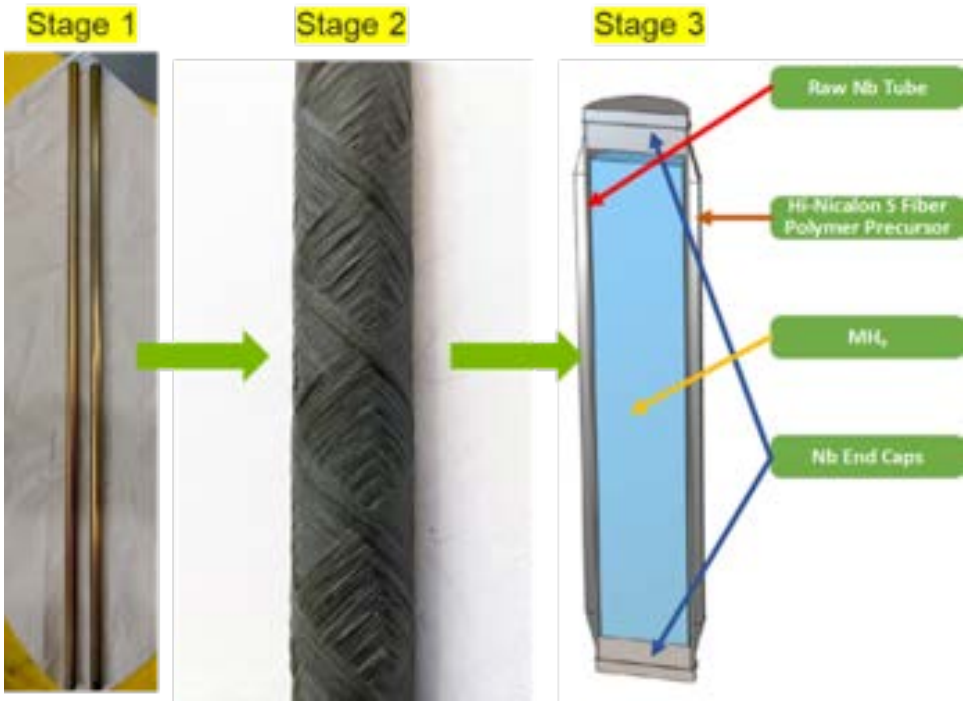

Figure 2: (a) Nb liners tubes coated with barrier coating, (b) Coated tubes enveloped with SiC composite. (c) Schematic of final form of the AMM ANL is developing.

Stage 1: Implementation of the H_2 permeation barrier on the Nb liners. At this stage, ANL employed advanced coating technologies to apply the barrier both inside and outside the small-diameter Nb tubes. (details in section 2.2)

Stage 2: Application of the ceramic matrix composite (e.g., SiC/SiC-based cladding) shell over the prepared coated Nb tubes. Argonne collaborated with Ceramic Tubular Products (CTP) to develop the SiC composite shell, which was then shrink-fitted over the coated Nb liners. (details in section 2.3)

Stage 3: Loading of YH_2-x pellets into the Nb + CMC shells prepared in Stage 2, followed by sealing both ends of the shells with Nb end caps welded to the liner structure. Argonne has partnered with LANL to produce the YH_2-x pellets, and the end caps were joined using TIG welding at ANL.

2.2. H_2 permeation barrier development for the Nb liners.

Based on our work carried out in previous year and this year in the microreactor program, we have identified that best performing permeation barrier design is a multilayer layer of

$CrAl/Al_2O_3$. This design has been primarily developed for TZM based moderators, but the barrier design is transferable to Nb based substrates with an addition of Al_2O_3 based substrates, more details regarding the material selection and thickness identification can be found in our previous report [7]. To recap the generated property details for this barrier coating, we have summarized the analysis in figure 3.

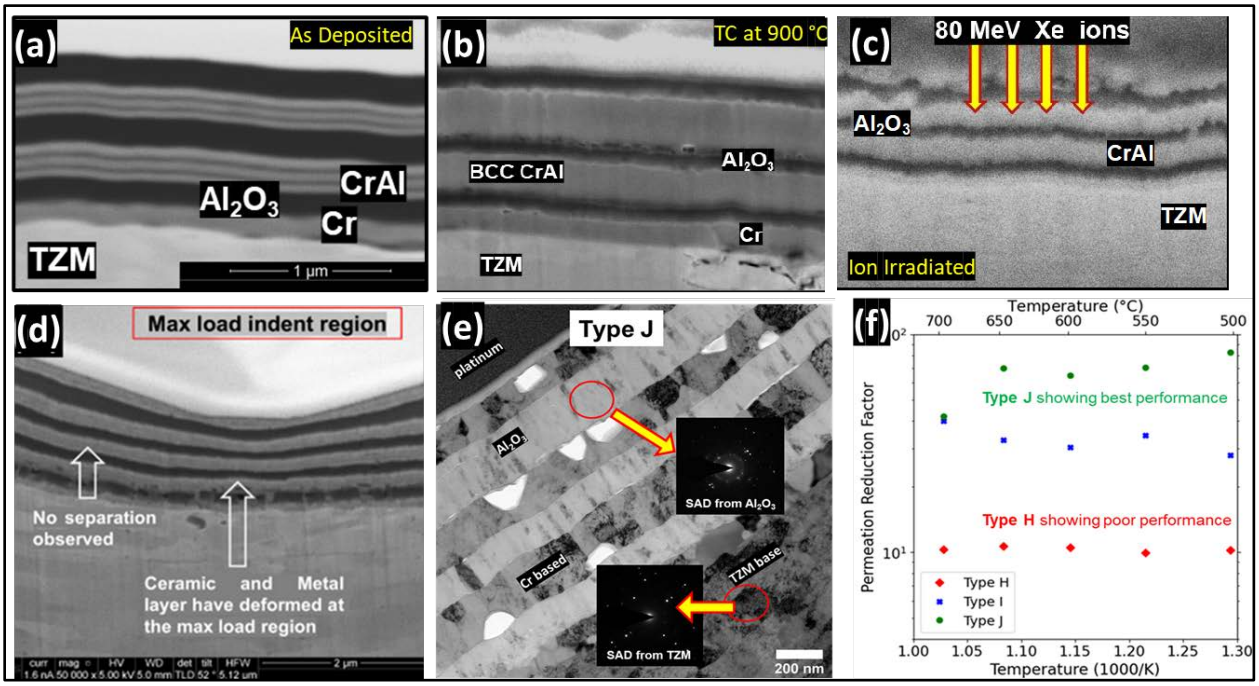

Figure 3: FIB cross sections of the best performing H_2 permeation barrier design (a) As prepared multilayer design, consisting of Cr-Al/Al_2O_3, (b) Status of the permeation barrier after undergoing 10 thermal cycling treatment at 900°C, (c) Status of the permeation barrier after high temperature (650°C) ion irradiation performed with 80 MeV Xe ions to achieve ~10 dpa damage, (d) The multilayer after it has been indented with a max force of 500gf showing local plastic deformation without any obvious failure observed, (e & f) TEM BF of the corresponding best performing multilayer design against high temperature (~700 °C) H_2 permeation (Type J, green plot, in figure (f)). The phases can maintain their respective phases, no hydride or amorphization in the microstructure is observed.

Figure 3 provides a detailed evaluation of the performance and robustness of the developed metal ceramic multilayer hydrogen permeation barrier design, composed of $CrAl/Al_2O_3$ layers (in this case shown over TZM substrate), under various conditions mimicking the extreme conditions expected within a reactor. The figure 3**(a)** shows the initial state of the multilayer design as prepared, highlighting the precise and uniform deposition of the $CrAl/Al_2O_3$ layers, achieved with ALD and PVD process. In figure 3**(b)**, the permeation barrier is shown after enduring ten thermal

cycles at 900°C, simulating the high-temperature fluctuations typical in gas cooled reactor environments. The structure maintains its integrity, indicating its resilience to repeated thermal stress. Figure 3**(c)** further assesses the barrier's durability by exposing it to ion irradiation at 650°C using 80 MeV Xe ions, replicating radiation damage equivalent to approximately 10 displacements per atom (dpa). The results show that the multilayer remains intact, demonstrating excellent radiation resistance, which is crucial for maintaining barrier performance in a nuclear reactor.

The mechanical stability of the barrier is then tested in figure 3**(d)**, where the multilayer is subjected to a maximum indentation force of 500gf for 15 secs. The material exhibits local plastic deformation without any signs of delamination or failure, confirming its mechanical robustness. Figure 3 **(e)** provide a closer examination through transmission electron microscopy (TEM), where the bright field (BF) images and selected area diffraction (SAD) patterns illustrate the structural integrity of the Al_2O_3 and CrAl layers even after exposure to hydrogen at 100 Kpa pressure at 700 °C. Figure 3 **(f)** shows the permeation reduction factor against temperature, where Type J design (seen in the TEM BF, figure (e)) emerges as the superior design, offering the best performance in reducing hydrogen permeation at high temperatures (~700°C) compared to other tested configurations.

This comprehensive evaluation highlights the CrAl/Al_2O_3 multilayer design's exceptional performance across thermal cycling, radiation exposure, and mechanical stress tests, making it a capable candidate for use as a hydrogen permeation barrier in high-temperature nuclear environments, particularly in advanced nuclear reactors.

2.3. SiC composite shell manufacturing and loading of coated Nb liners inside it.

Argonne is collaborating with Ceramic Tubular Products LLC (CTP) to develop the necessary SiC composite outer shells that will house the coated Nb liners. CTP, recognized for its expertise in advanced ceramics, specializes in producing SiC-SiC composites known for their resilience in high-temperature environments, combining the strength and thermal stability of SiC with the enhanced toughness provided by SiC fibers. The manufacturing process leverages polymer impregnation and pyrolysis (PIP) [8] , a liquid infiltration technique that begins with the fabrication of a SiC fiber preform over graphite mandrels through braiding, weaving, or stacking

multiple layers of SiC-based fabrics into the desired configuration. As depicted in Figure 4 (a), CTP has braided beta-phase SiC fibers over ~9.5 mm OD graphite mandrels to match the ID of the coated Nb liners, followed by the deposition of a layer of pyrolytic carbon over the braiding to enhance bonding with the PIP SiC matrix.

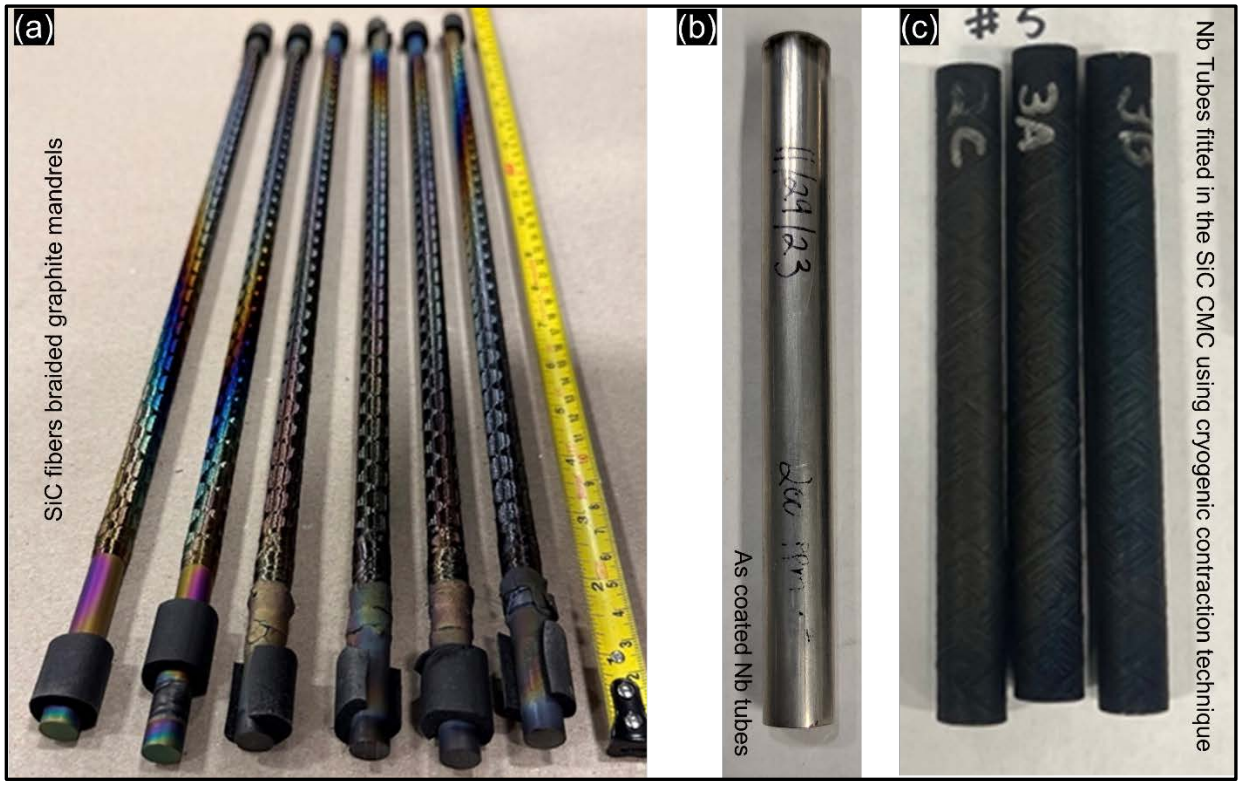

Figure 4: (a) SiC fibers braided graphite mandrels (~50 cm long) after going through the process pyrolytic carbon coating to generate a layer of carbon over the fibers for better bonding with PIP SiC matrix. Picture credit CTP LLC. (b) 10 cm long, as coated Nb tube sections shipped to CTP & (c) 10 cm long coated Nb tubes shrink fitted within SiC CMC shells.

The preform is then impregnated with a specially chosen polymer precursor, such as polycarbosilane, using techniques that ensure thorough infiltration of the polymer into the fiber architecture, potentially involving vacuum or pressure. Following impregnation, the preform is dried to ensure uniform distribution of the polymer, which adheres seamlessly to the SiC fibers while eliminating any volatile constituents. Next, the polymer-infused preform undergoes pyrolysis in a controlled environment, where the polymer precursor decomposes and gradually transforms into SiC. CTP meticulously controls the pyrolysis parameters, including temperature, rate, and duration, to optimize the purity and quality of the resulting SiC matrix. To achieve a

densely packed SiC matrix and minimize residual porosity, the impregnation and pyrolysis processes are repeated multiple times. Each iteration enhances the composite's density and mechanical properties, resulting in a dense SiC-SiC composite. The SiC fibers impart crack propagation resistance and toughness, while the SiC matrix provides rigidity and strength. This synergy between the matrix and fibers enhances the composite's durability, enabling the SiC shell to remain robust and resilient, even in the face of the extreme conditions expected in its application.

The SiC shells generated by CTP need to be fitted over the 10 cm long coated Nb tubes (as shown in Figure 4(b)). These SiC shells offer structural support, thermal stability, and protection against external environmental factors, while the Nb liner serves as a hydrogen-permeation barrier within the composite assembly. CTP employed a cryogenic contraction technique to fit the metal Nb tube within the ceramic composite shell. This shrink-fitting process involves cooling the Nb tubes to cryogenic temperatures, causing them to contract and allowing for a snug fit within the SiC shells. As the assembly returns to room temperature, the Nb liners expand, ensuring they are securely encapsulated within the SiC CMC structure. The effects of cryogenic temperatures on the coating and the impact of Nb liner contraction are detailed in a previous report [7]. The final result of the shrink-fitting process is shown in Figure 4(c), where the SiC shell flushes with the Nb tubes..

In summary, figure 4 illustrates the critical steps in the fabrication of a composite structure that combines SiC fibers, pyrolytic carbon coating, a PIP SiC matrix, and a coated Nb liner. Each component and processing step contributes to the overall durability, functionality, and performance of the final advanced moderator module intended for use in demanding nuclear environments.

2.4. Joining the Nb end caps with the AMM shells.

Figure 5 provides a detailed representation of the SiC CMC shell used in the Advanced Moderator Module (AMM) design, highlighting its structural components and the critical welding areas necessary for sealing the assembly. Figure 5 (a) illustrates a schematic of a 10 cm section of the SiC CMC shell, which encapsulates the Nb liner within, that is received from CTP, also shown in figure 4 (c). Figure 5 (b) shows an engineering drawing of the AMM shell, detailing the cross-sectional dimensions and specific regions where welding is required. The drawing provides a comprehensive view of the shell's structure, with particular attention to the Nb end caps at both ends of the shell. These caps need to be welded in place (identified in the drawing) to create a

hermetic seal not only against H_2 loss, ensuring that the interior of the AMM remains isolated from external conditions, which is vital for not only maintaining the integrity of the metal hydride (YH_{2-x}) but for the hydrogen-permeation barrier too.

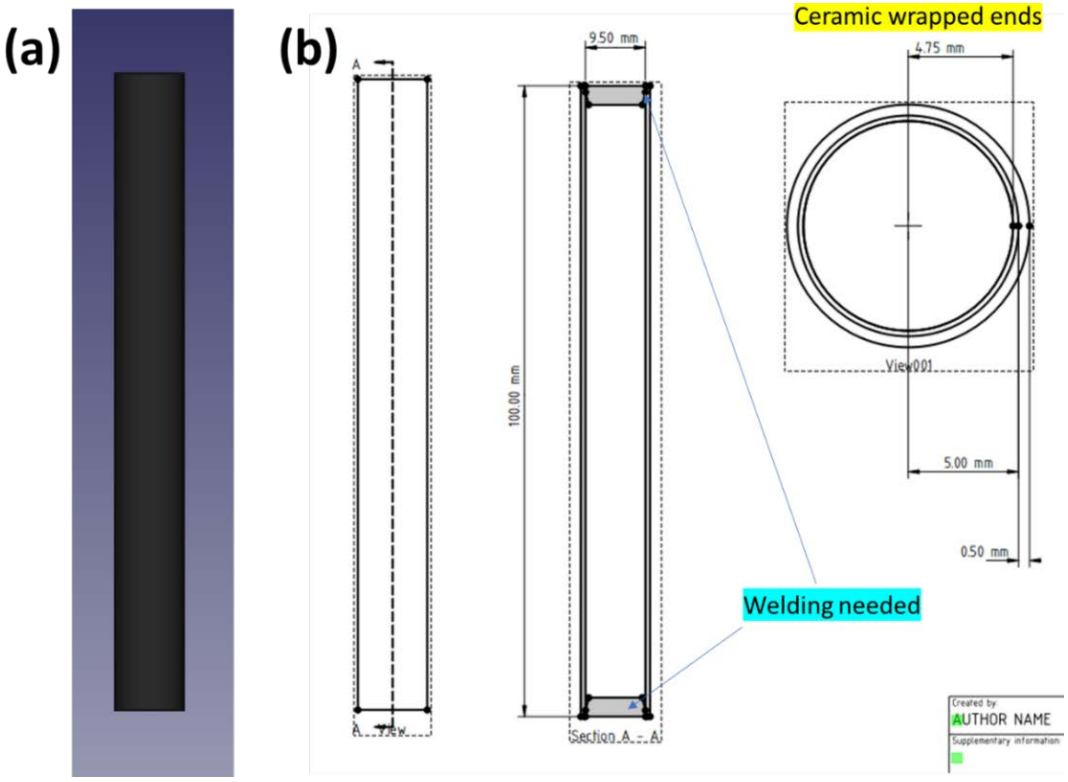

Figure 5: (a) Schematic of the small 10 cm section of the SiC CMC shell enveloping a Nb liner within. (b) Engineering drawing with dimensions of the AMM shell cross section, displaying the Nb end caps on both ends, welded to create the hermetic seal.

` To achieve the welding, Tungsten Inert Gas (TIG) welding has been used. TIG welding, also known as Gas Tungsten Arc Welding (GTAW) [9], is a welding process that uses a non-consumable tungsten electrode to produce the weld. The electrode is housed in a torch, which directs the welding arc onto the workpiece, figure 6 (a). An inert shielding gas, typically argon, helium, or a mixture of the two, is used to protect the weld area from atmospheric contamination. This shielding gas is crucial in preventing the intrusion of oxygen, nitrogen, and hydrogen into the weld pool, which could otherwise cause weld defects such as porosity, cracking, and embrittlement. The specialized TIG welding setup at ANL features a sophisticated welding

chamber equipped with a protective glove box. This design ensures that the welding process occurs in a controlled atmosphere, protecting the weld from atmospheric contamination, which is crucial when welding reactive metals like Nb. Copper chillers designed for holding the AMM shells have been specially made, figure 6 (a). These chillers are critical in managing the heat generated during welding, preventing overheating of the niobium tube and ensuring that the weld area cools rapidly and evenly, which helps to maintain the integrity and strength of the weld and helps to reduce the heat affected zone (HAZ) to a minimum.

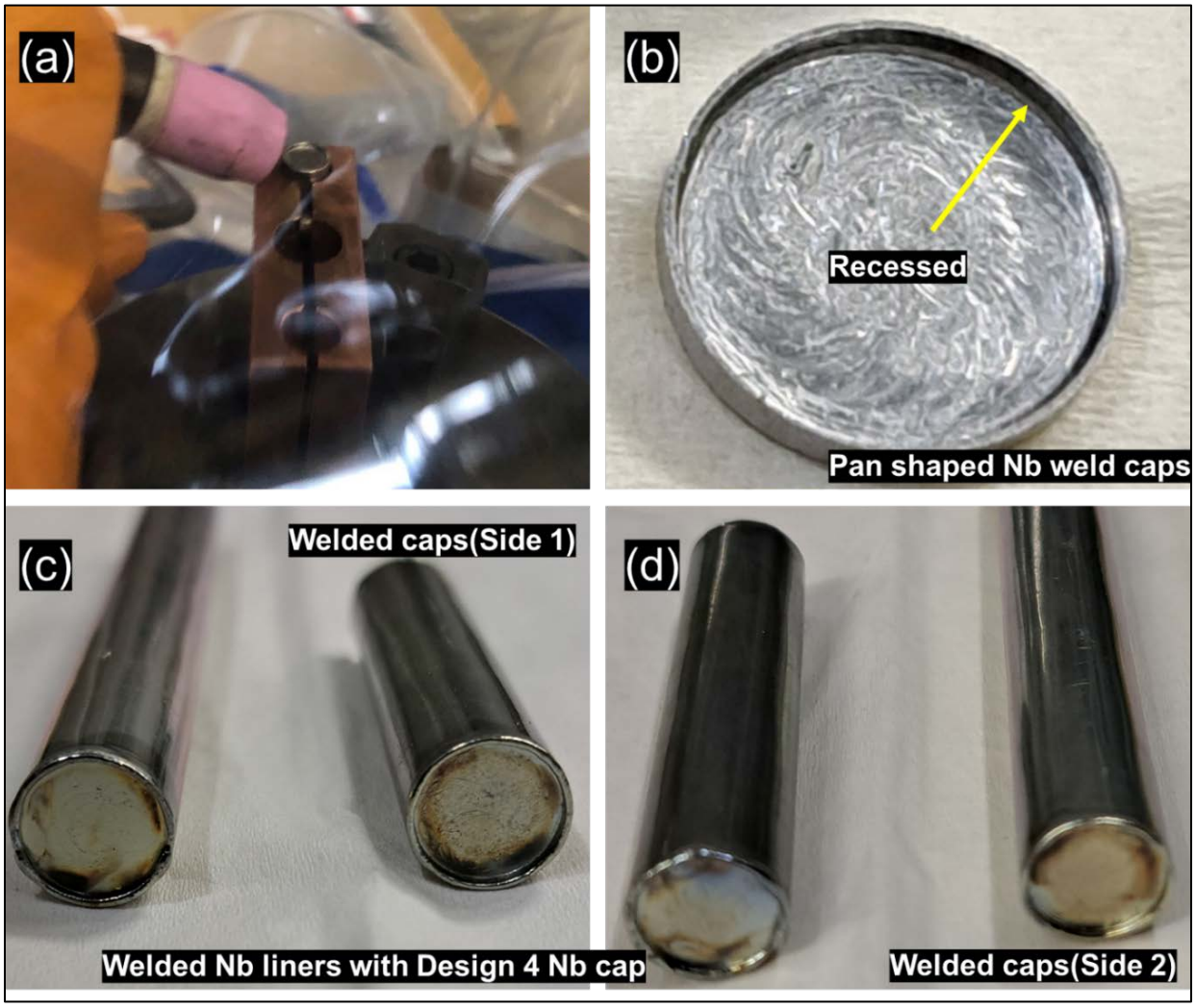

Figure 6: This figure illustrates the process and results of welding pan-shaped niobium (Nb) caps onto liners using the TIG welding technique (a) This image shows the TIG welding setup in progress, where a niobium cap is being welded onto a liner, (b) This close-up image displays a pan-shaped niobium weld cap, highlighting the recessed area within the cap to generate a secure

and consistent weld joint. (c & d) These image shows the final state of two Nb liners after completion of TIG welding with clean region of welded caps.

After every welding step a helium leak check is performed as a critical quality control step to ensure the integrity of welded Nb sample tubes. This procedure, conducted under the Central Shops at ANL, involves a meticulous process designed to detect even the smallest leaks in the welded joints of the niobium tubes. The acceptance criteria for this test are stringent, with any helium detection above 1.0×10^{-9} cc/sec considered unacceptable. Based on the visual results, figure 6 (c, d) was found after the welding process is completed, the welds are clean and well-formed, with no visible signs of defects such as cracks, voids, or excessive oxidation. Figure 6 (d) shows the niobium tube after the TIG welding process. The weld seam is visible, demonstrating the precision and quality achieved through this method. The clean, uniform welded seam indicates that the identified heat input and gas shielding have led to clean, smooth surfaces of the welded areas indicate that the TIG welding process was successful in achieving a high-quality welding.

In summary, the materials and methods outlined above establish the foundation for the fabrication of complete AMM assemblies at Argonne. The integration of multilayer $CrAl/Al_2O_3$ hydrogen permeation barriers, the development of robust SiC composite shells through close collaboration with industry partners, and the precision joining of niobium end caps together constitute a carefully engineered approach to ensure long-term performance in demanding reactor environments. While each of these steps, liner coating, composite cladding, and cap welding contribute to the overall success of the AMM design, our recent investigations have revealed that the end-cap regions represent the most performance-limiting factor due to the disproportionate hydrogen loss associated with niobium's high permeability. This finding has motivated a shift in emphasis from general shell fabrication to the systematic evaluation of end-cap coating architectures. Accordingly, the following sections present the manufactured AMM with varying end cap coating designs, which we compare the hydrogen retention performance presented in the results section of the report.

3. Experimental & development details:

3.1. Successful Fabrication of Complete AMM Modules.

Building upon the foundation described in the Materials and Methods section, we have, for the first time, successfully manufactured Advanced Moderator Modules (AMMs) fully loaded with yttrium hydride (YH_{2-x}) pellets. Figure 7 (a–c) illustrates the stepwise assembly and final form of these modules. The schematic in Figure 7 (a) highlights the overall AMM geometry, showing the Nb liner, SiC CMC shell, and welded Nb end caps. Figure 7 (b) provides photographic evidence of completed modules: the AMM shell with the YH_{2-x} pellets prepared separately, and the final sealed module with niobium caps welded in place. Figure 7 (c, c′, c″) shows close-up views of the end-cap regions after TIG welding and subsequent recoating, highlighting the uniform surface coverage critical for ensuring hermeticity and suppressing hydrogen permeation through the end caps.

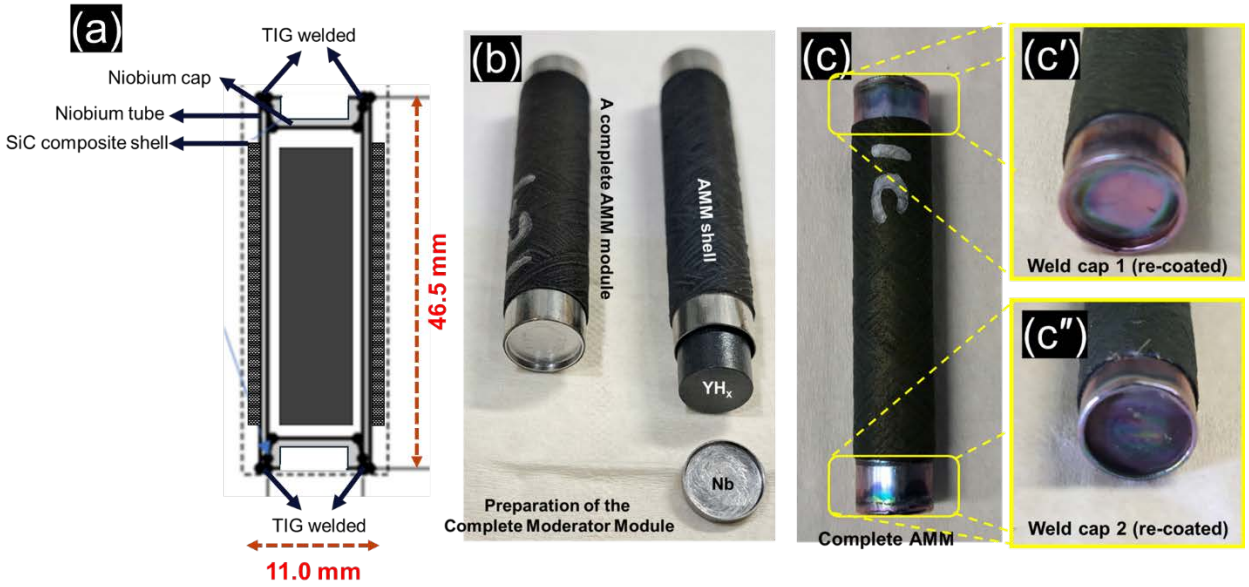

Figure 7: Successful fabrication of complete AMM modules with YH_{2-x} pellet loading., (a) Schematic of AMM design showing liner, CMC shell, and welded Nb end caps. (b) Fabricated AMM shells, YH pellets, and complete welded modules. (c, c′, c″) Close-up images of welded and re-coated Nb end caps, showing successful sealing.

In addition to fabricating short modules for initial proof-of-concept demonstration, we have also scaled the process to generate varying-length AMM modules, shown in Figure 8 (a–b). These include modules of lengths 5 cm, 10 cm, and 50 cm, demonstrating the scalability of the fabrication process. The results confirm Argonne's capability to manufacture AMM modules up to 1 m long and 45 mm in outer diameter (OD). The ability to fabricate modules of different lengths is a critical

step toward future deployment, as it provides flexibility in reactor design integration, scalability of moderator volume, and testing under varying irradiation environments.

This marks a major milestone in AMM development, as it transitions the technology from individual component fabrication (liners, coatings, SiC shells, weld caps) to the demonstration of complete, sealed, and functional moderator modules. These fabricated AMMs have been used for performance validation studies for understanding their hydrogen retention measurements.

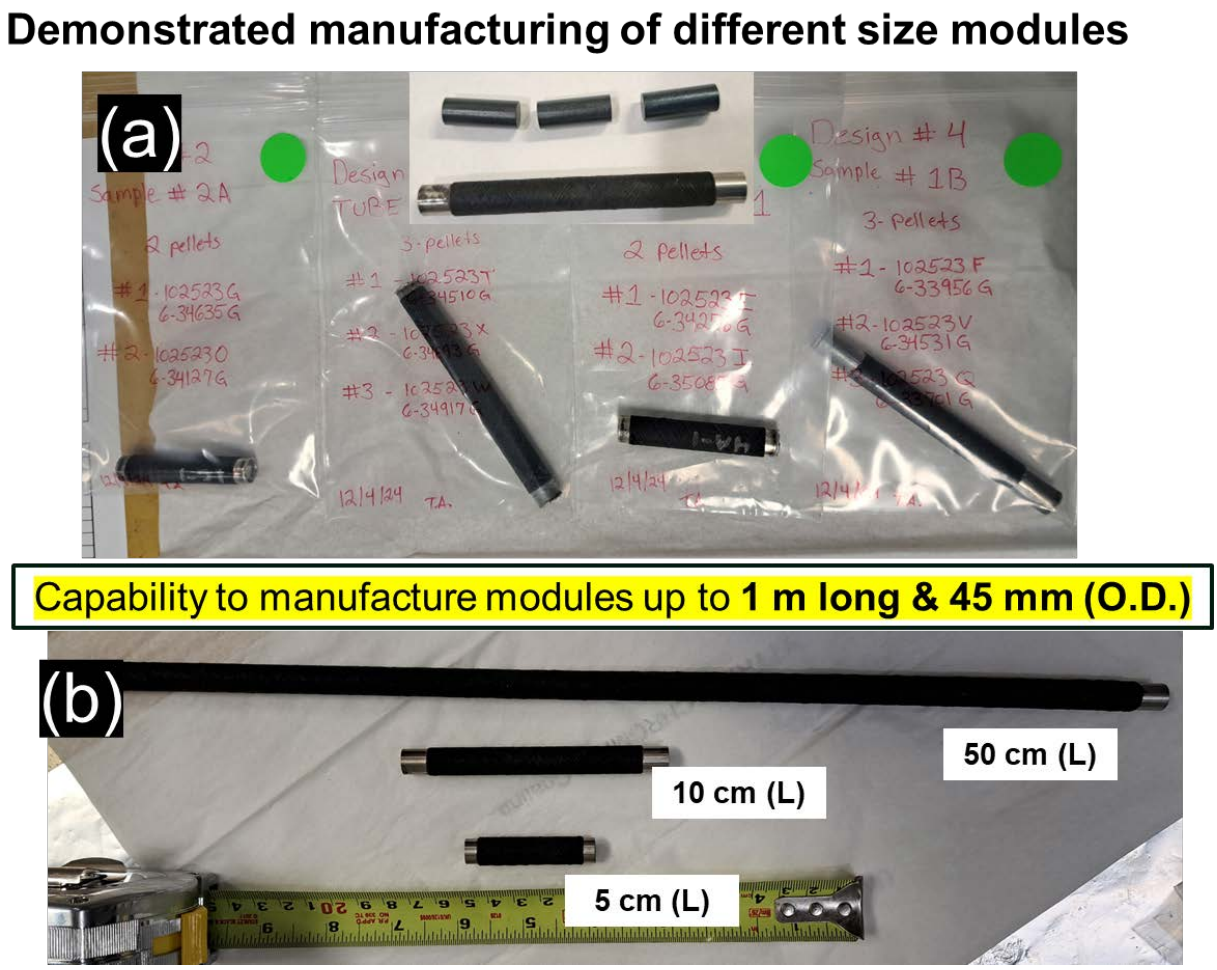

Figure 8: Scalability of AMM fabrication process. (a) Fabricated AMM modules of varying lengths (5 cm, 10 cm, 50 cm). (b) Demonstration of Argonne's capability to manufacture AMM modules up to 1 m in length and 45 mm OD.

3.2. Confirmation of hermetic sealing of the AMM module using X-ray CT characterization of AMM Modules:

To validate the hermetic integrity and structural soundness of the fabricated AMM modules, X-ray computed tomography (CT) scans were performed on one of the modules shipped

to LANL. The X-ray CT imaging provides a non-destructive method to detect internal defects such as cracks, voids, or weld discontinuities in the end caps, liner, or welded joints. Such analysis is essential to confirm the absence of leakage pathways and to establish confidence in the module's long-term hydrogen retention capability. As shown in Figure 9 (a–c), the CT cross-sectional images taken from multiple perspectives reveal no visible defects in the weld seam, end-cap geometry, or liner interface. The high-resolution scans confirm that the AMM module exhibits excellent weld quality and maintains the structural continuity required for hermetic sealing. These findings provide concrete proof that the fabricated module meets the strict requirements for hydrogen containment and validates the robustness of the developed AMM manufacturing approach.

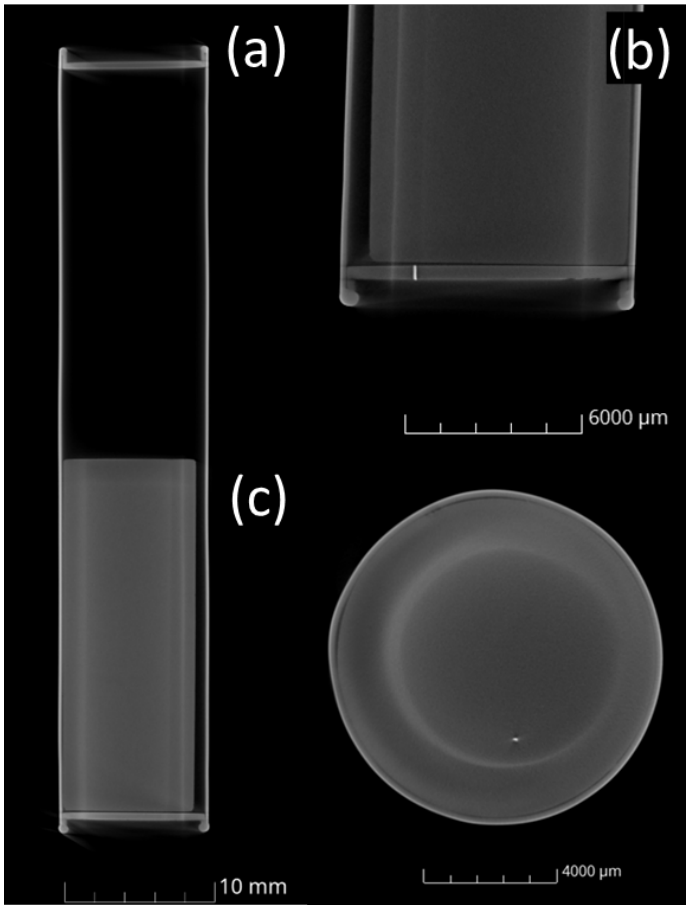

Figure 9: X-ray CT analysis of a fabricated AMM module shipped to LANL. (a) Longitudinal cross-section showing the internal pellet loading and end-cap closure. (b) Enlarged view of the welded end-cap region. (c) Top-down cross-section through the cap showing uniform weld and liner integrity.

3.3. End cap surface engineering after welding.

One of the most critical challenges in Advanced Moderator Module (AMM) fabrication is the treatment of the niobium (Nb) end caps following welding. While the cylindrical liner can be uniformly coated with hydrogen permeation barriers during early processing steps, the end caps are introduced at the final assembly stage, after pellet loading and sealing. The welding process, though necessary to achieve hermetic closure, locally damages or removes the protective barrier coating, leaving the end-cap surfaces highly vulnerable to hydrogen permeation. Given the intrinsically high hydrogen permeability of Nb, these small uncoated areas can become the dominant leakage pathways, significantly undermining the retention capacity of the entire AMM module.

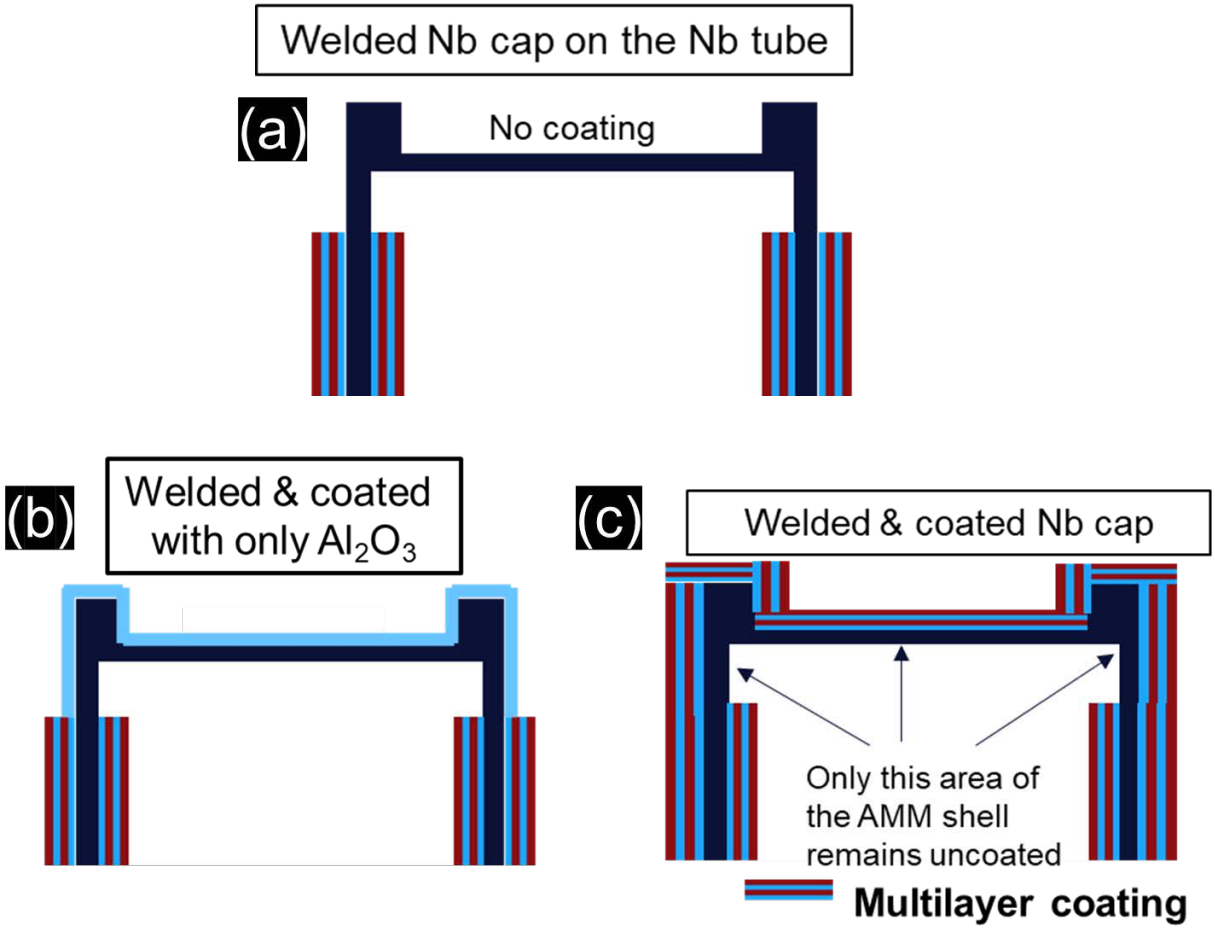

Figure 10: Schematic of end-cap coating strategies after welding. (a) After Nb cap welding is completed, (b) Single-layer design (0.5 µm Al_2O_3). (c) Intermediate multilayer architectures (1.2–1.8 µm) with only the weld groove region left uncoated, highlighting the recoating approach for restoring barrier continuity at the welded end caps.

The end-cap surface area is relatively small compared to the cylindrical liner, its contribution to overall hydrogen loss is disproportionately large if left insufficiently coated (discussed more in the discussion section of the report). To address this issue, we have developed a systematic end-cap surface engineering approach, whereby different coating designs were re-applied after welding. As illustrated in Figure 10 (a–c), the strategy involves recoating the weld-affected zones of the end caps to restore barrier continuity and minimize hydrogen leakage. Several coating designs were investigated, ranging from single-layer alumina films to multilayer architectures with varying total thickness:

- **Single-layer 0.5 µm Al_2O_3**: A baseline design that is simple and rapid to deposit, but needs to be validated at 750 °C. This will be the easiest approach in terms of manufacturing economics.
- **Intermediate multilayers (1.2–1.8 µm)**: Alternating Cr/Al_2O_3 stacks that introduce compliant interfaces to redistribute stresses if the single layer approach fails.

By implementing optimized coatings after welding, it is possible to restore barrier performance without the need for complex welding modifications. This simplified, post-weld recoating strategy not only ensures the hydrogen retention performance of the AMM is preserved, but also streamlines the manufacturing process, saving both time and cost. The ability to apply reliable coatings directly to the end caps after welding provides a practical pathway to scale-up, enabling consistent fabrication of AMM modules that can withstand long-duration, high-temperature operation in nuclear reactor environments.

To achieve this goal, we have similarly utilized ALD only for the single layer barrier and ALD and PVD processes to implement the multilayer over the welding regions. The Nb cap regions were first cleaned using 0.05 M HF and then washed with acetone and ethyl alcohol. For Al_2O_3 ALD growth, the cleaned Nb tubes were maintained at 150–180 °C to reduce H_2 diffusion within the alumina matrix, usually a byproduct of the deposition process.

For the CrAl coating the innovative magnetron plasma-based sputter coating system, at ANL has been used which is tailored to apply metal coatings on the exterior surfaces of complicated substrates. The AMM welded shells, which initially undergo a cleaning process using acid and acetone, are further purified using a secondary plasma application. Typically, the deposition rates stand at roughly 5 nm/s for Cr and double that for Al at 10 nm/s. The final

deposition thickness spans from ~0.2 to 0.5 μm. To guarantee precision, these deposition rates are validated by analyzing coatings on Si wafers and later directly over the Nb welded caps through a cross-sectional examination with a scanning electron microscope.

3.4. Contribution of SiC CMC De-Gassing to Measured Weight Loss.

During high-temperature exposures of AMMs, it is critical to distinguish between hydrogen mass loss originating from the YH_{2-x} pellets and other potential contributors within the assembly. One such contributor is the SiC ceramic matrix composite (CMC) shell, which is used to reinforce the niobium (Nb) liner. While the SiC/SiC composite provides structural rigidity, thermal stability, and compatibility with high-temperature reactor environments, it is also known to exhibit initial de-gassing behavior when exposed to elevated temperatures. This phenomenon arises from the release of residual species (e.g., trapped gases, carbonaceous phases, or processing-related volatiles) within the CMC during early thermal cycling.

To quantify this effect, dedicated thermal exposure experiments were conducted on SiC CMC shells of varying lengths. Figure 11 presents both a representative image of the SiC CMC shell (left) and the measured weight loss versus time for two different shell lengths: 67 mm and 36.5 mm. The weight-loss behavior follows an exponential decay trend, with the majority of mass loss occurring within the first 200 hours at 750 °C, after which the curves asymptotically approach a plateau. Importantly, longer SiC shells exhibit proportionally higher de-gassing contributions, consistent with greater exposed volume of composite material.

These results demonstrate that a fraction of the measured weight loss in SiC-wrapped AMM modules cannot be attributed solely to hydrogen release from the YH_{2-x} pellets. Instead, part of the signal arises from intrinsic CMC de-gassing, which, if uncorrected, would lead to overestimation of hydrogen loss and underestimation of the H/Y ratio retention in the pellet. Therefore, all weight-loss data presented in the results section for coated AMM modules will be corrected by subtracting the baseline de-gassing contribution established here. By normalizing against the measured de-gassing rates of CMC-only shells of similar dimensions, we ensure that the reported hydrogen retention values more accurately reflect the true performance of the AMM barrier coatings and end-cap designs.

This correction framework strengthens the reliability of the reported results, particularly when comparing different coating architectures, end-cap treatments, or environmental conditions (vacuum vs. Ar). The methodology also highlights the importance of accounting for non-hydride-related contributions when interpreting mass-loss data in complex, multi-material systems such as AMMs.

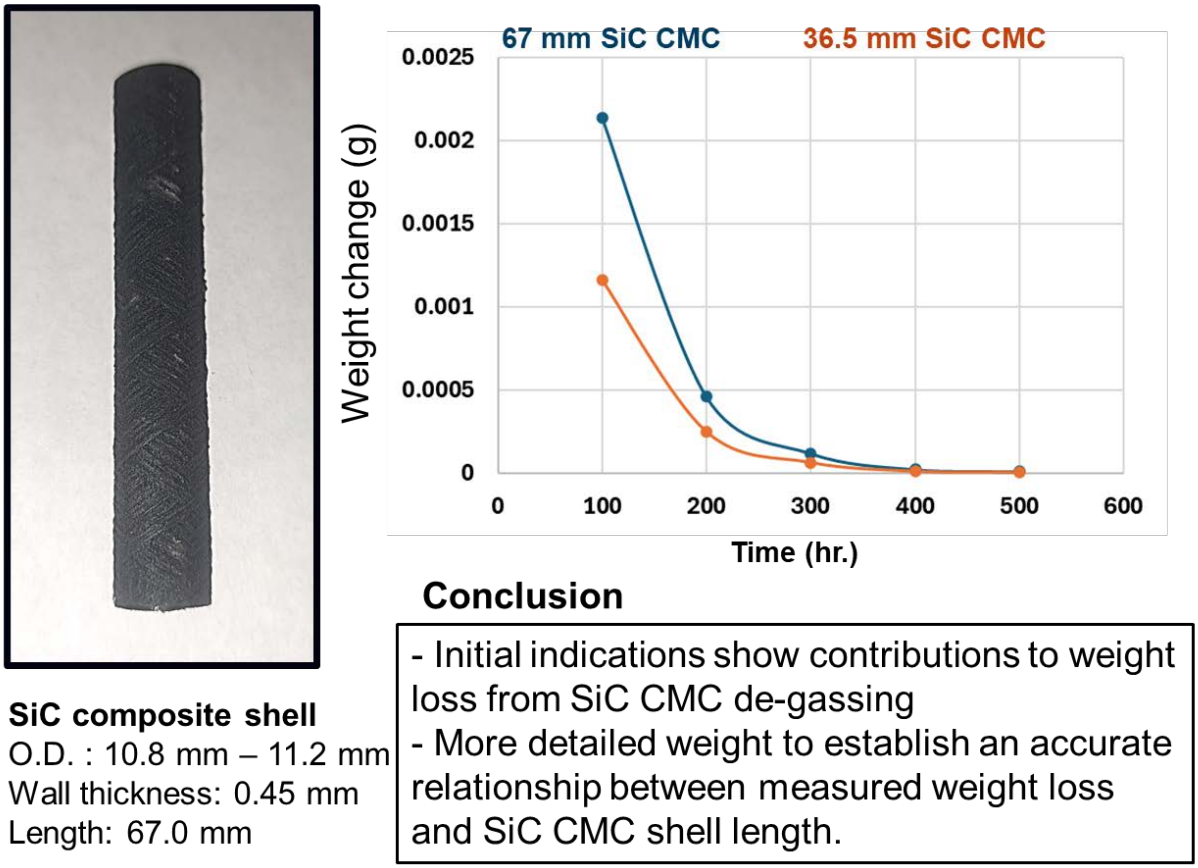

Figure 11: Representative SiC CMC shell (left) and measured weight-loss kinetics during de-gassing at 750 °C (right). Data are shown for two shell lengths (67 mm and 36.5 mm), indicating higher de-gassing contributions for longer shells. These results provide baseline correction factors for isolating true hydrogen loss from YH_{2-x} pellets in AMM modules.

3.5. Application of optimized H_2 permeation barrier generated over Niobium liner surface for all studied AMM modules.

To ensure consistent baseline performance across all AMM modules evaluated in this study, an optimized hydrogen permeation barrier coating was uniformly applied to the inner and

outer surfaces of the niobium (Nb) liners prior to end-cap welding and final module assembly. This approach was deliberately selected so that differences in hydrogen retention performance across the modules can be attributed specifically to the variations in end-cap coating architectures, rather than inconsistencies in the liner coating. The permeation barrier design employed consists of an alternating multilayer architecture of Cr and Al_2O_3, developed at Argonne National Laboratory. This design was identified in prior studies as one of the most effective configurations for suppressing hydrogen transport under high-temperature conditions (≥700 °C).

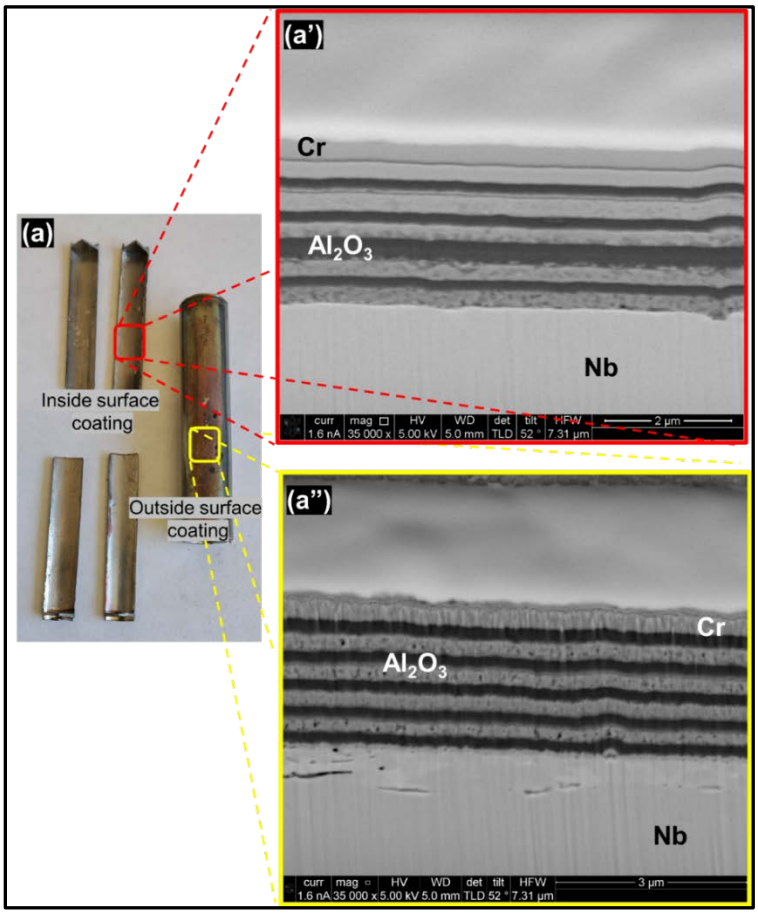

Figure 12: A detailed analysis of the coating layers on the inside and outside surfaces of niobium (Nb) tubes used for doing further thermal studies. (a) The tube is cut to reveal the internal and external coating cross-sections on the tube surfaces. (a') FIB cross section of the inner surface area marked with red box, showing the developed $CrAl/Al_2O_3$ multilayer and (a") FIB cross section of the outer surface area marked with yellow box, showing the developed $CrAl/Al_2O_3$ multilayer.

As shown in Figure 12 (a′ and a″), cross-sectional SEM images confirm the high structural quality of the multilayers deposited on Nb substrates. The films display:

- Sharp and uniform interfaces between Cr and Al_2O_3 layers, critical for maximizing diffusion path tortuosity and reducing effective hydrogen permeability.
- Conformal coverage across the Nb liner surface, with excellent adhesion and minimal interfacial defects.
- Stable nanolayer stacking, with total thicknesses of ~3.4 μm.

The inside surface of the liner (facing the YH_{2-x} pellet) and the outside surface (exposed to the SiC CMC shell) were coated under identical deposition conditions, ensuring that both sides of the Nb liner function as hydrogen-impermeable barriers during operation. All AMM modules tested in this campaign employed the same optimized liner coating, the impact of the coating on liner performance can be considered fixed and reproducible across all samples. This design choice provides two critical benefits:

- **Isolation of End-Cap Effects**: Since liner coating performance remains constant, the comparative analysis of hydrogen retention can focus exclusively on the contribution of the end-cap regions, which are otherwise the dominant pathways for hydrogen leakage due to bare Nb permeability.
- **Assurance in Liner Integrity**: The use of this optimized coating assures that the cylindrical liner itself does not represent a limiting factor in AMM performance. Any hydrogen loss observed in long-duration thermal exposures can therefore be traced to the end caps and their associated coating architectures.

4. Results.

4.1. Thermal Testing of AMM Modules with Varying End-Cap Coatings.

To evaluate the H_2 loss and long-term stability of the Advanced Moderator Module (AMM) encapsulation design, a series of thermal exposure experiments were carried out on fully fabricated AMM assemblies incorporating different end-cap coating architectures. Modules were sealed with TIG-welded niobium end caps, which were subsequently re-coated to restore a hermetic hydrogen

barrier. The tested coating configurations ranged from single-layer 0.5 μm Al_2O_3 coatings to multilayer stacks up to 3.2 μm thickness (8 layers, alternating Cr/ Al_2O_3 films). These coatings were introduced to mitigate hydrogen loss through the Nb end caps, which represent critical weak points in the overall hydrogen barrier due to niobium's intrinsically high hydrogen permeability. By systematically varying coating thickness and design, the relative contribution of the end-cap region to hydrogen retention is isolated and quantified. Thermal exposures were performed under the following environments:

(a) **High vacuum (~5×10^{-6} mbar) at 750 °C:** This represents an aggressive outgassing scenario, maximizing the chemical potential gradient for hydrogen transport. The vacuum condition subjects the coatings to tensile stress states, making it a critical environment for assessing coating adhesion, spallation resistance, and hydrogen permeation performance.

- AMMs with 500 nm, 1μm, and 3.2 μm coating on the end caps were tested under those conditions, tested at Argonne.

(b) Flowing Argon (> 1 ATM pressure, 50 sccm flow) environment at 750 °C: This environment simulates inert gas operation in microreactors, where moderate convective removal of hydrogen occurs but external pressure provides a more compressive stress state within the coatings. This comparison highlights how stress state (tensile vs. compressive) directly influences coating permanence and crack formation. .

- AMMs with 500 nm, 1μm, and 3.2 μm coating on the end caps were tested under those conditions, tested at Argonne.

(c) High vacuum (~5×10^{-6} mbar) at 800 °C, tested at LANL: These exposures push the AMM design closer to operational limits and probe high-temperature degradation modes. The increased thermal mismatch between Nb and ceramic layers at 800 °C amplifies coating stresses, thereby providing critical insights into the stability margins of each end-cap design.

- AMMs with 1.2 μm coating on the end cap, tested at LANL.

4.2. Performance of AMM modules with 500 nm Al_2O_3–coated Nb end caps under Argon and Vacuum environments.

To evaluate the role of thin single-layer coatings, AMM modules (Figure 13) sealed with Nb end caps coated with 500 nm Al_2O_3 were fabricated and tested under two representative

environments: **(i)** Argon (1 atm, 50 sccm flow) and **(ii)** high vacuum (~5×10^{-6} mbar). The purpose of these studies was to establish the lower performance bound of minimalistic coating architectures..

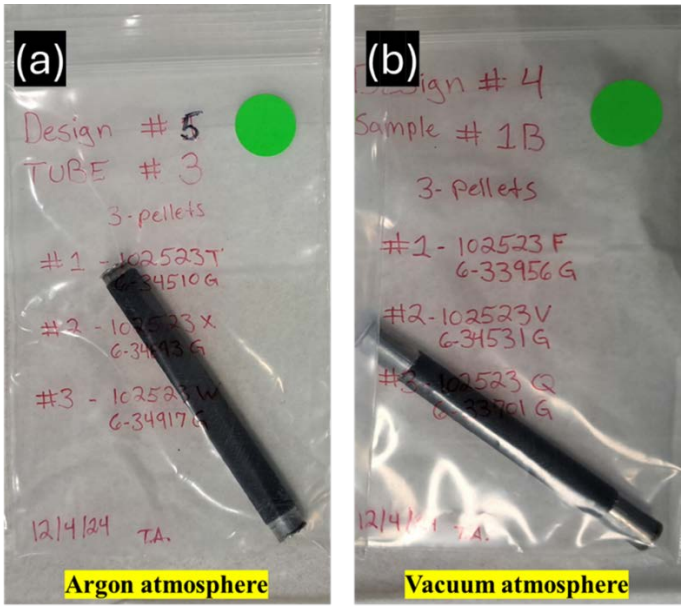

Figure 13. Photographs of tested AMM modules with 500 nm Al_2O_3–coated end caps prior to thermal testing: (a) Argon-tested module and (b) vacuum-tested module.

As shown in **Figure 14**, the measured H/Y ratio evolution reveals that both cases suffered significant hydrogen loss over the 500-h test interval at 750 °C. Specifically, the vacuum-exposed module lost approximately **21%** of the initial hydrogen content, while the Argon-tested module exhibited a slightly smaller but still severe loss of **18%**. Under vacuum, the mass loss measured per 100 hours follows an almost linear trend. In contrast, under Argon, the initial rate of H_2 loss was much lower than in vacuum, but after ~300 hours the mass loss accelerated. The corresponding weight loss trends confirmed that thin Al_2O_3 coatings are insufficient to suppress H_2 permeation through the Nb end caps, irrespective of the external environment. While both atmospheres produce notable degradation, the results demonstrate a clear trend: vacuum conditions exacerbate hydrogen release due to the steeper pressure gradient across the cap region. Nevertheless, the difference between argon and vacuum exposures was not sufficient to render the 500 nm Al_2O_3 coating a viable solution. These findings underscore the necessity of employing **multilayer architecture with multilayer architecture and higher thickness,** for expected coating stability.

Overall, this study highlights that although thin single-layer Al_2O_3 coatings provide a simplified processing route, their inability to limit hydrogen permeation, even in inert Argon conditions, makes them unsuitable for AMM deployment. This further validates the strategy of optimizing multilayer designs for end-cap coatings, as end caps disproportionately contribute to H_2 leakage due to Nb's intrinsic high permeability.

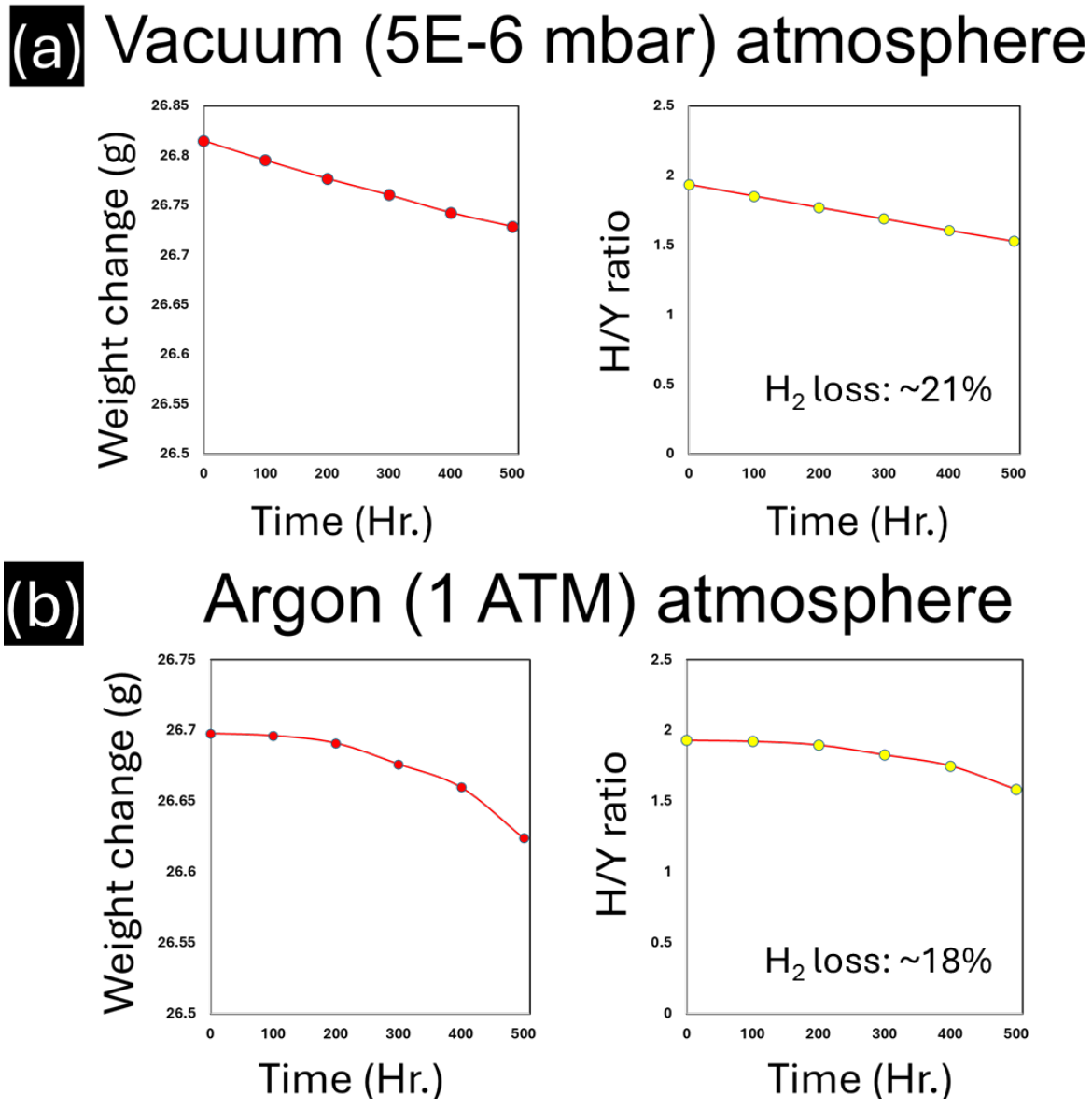

Figure 14. Measured H/Y ratio evolution for AMM modules with 500 nm Al_2O_3–coated Nb end caps tested at 750 °C. (a) Argon (1 atm, 50 sccm flow) and (b) vacuum (~5×10^{-6} mbar). Both cases show substantial hydrogen loss, with ~21% loss in vacuum and ~18% loss in Argon, confirming that single-layer coatings are insufficient for H_2 retention.

4.2.1. Evolution of YH_{2-x} Pellet Appearance after AMM Exposure.

The visual inspection of yttrium hydride (YH_{2-x}) pellets before and after AMM thermal exposure provides important qualitative insights into hydrogen retention and stability. As shown in Figure 15, the as-prepared pellet (a) exhibits a uniform dark blue coloration, which is characteristic of near-stoichiometric YH_{2-x} compositions. This blue tint originates from hydrogen-induced electronic states within the Y–H lattice that strongly affect optical absorption.

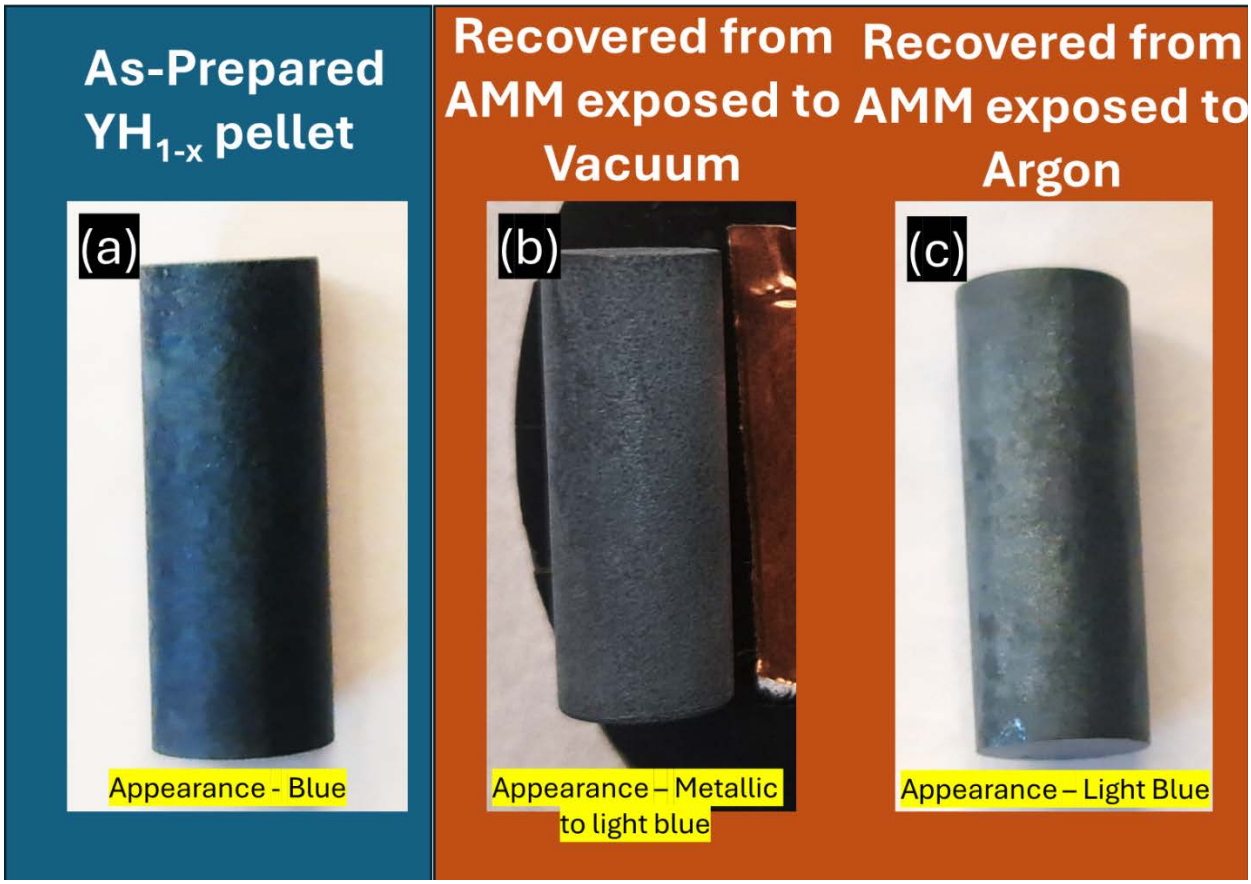

Figure 15. Optical appearance of YH_{2-x} pellets: (a) as-prepared pellet showing the characteristic blue color of YH_{2-x}, (b) pellet recovered from AMM tested under vacuum with 500 nm coated end cap, exhibiting metallic gray/light-blue surface due to severe hydrogen loss, and (c) pellet recovered from AMM tested under argon, retaining a lighter blue shade indicative of partial hydrogen retention.

After thermal testing in the AMM under vacuum conditions, the recovered pellet (b) displayed a distinct shift toward a metallic gray-to-light blue appearance. This change indicates substantial hydrogen loss (~21% as quantified in mass-loss data), resulting in partial

decomposition toward metallic yttrium or sub stoichiometric YH_{2-x} phases. The diminished hydrogen occupancy reduces the optical bandgap contribution of hydride phases, causing the pellet to appear more metallic. In contrast, the pellet recovered from the argon atmosphere exposure (c) retained a lighter blue coloration. While this still suggests measurable hydrogen loss (~18%), the extent of dehydrogenation is less severe than in vacuum. The residual hydride phases preserve some of the characteristic blue absorption, though the lighter tone reflects a reduction in hydrogen content relative to the as-prepared state.

Importantly, despite these losses, the AMM modules demonstrated hermetic integrity throughout the exposures. No oxidation products or surface discoloration consistent with oxygen ingress were observed, and no weight gain was detected in the post-test analyses. This indicates that the AMM shells remained sealed against external contaminants, and the observed hydrogen loss arises solely from permeation through the Nb liner and coating system, rather than from atmospheric leakage or oxidation reactions.

The overall color evolution from blue to metallic gray (vacuum) / light blue (argon) directly correlates with hydrogen stoichiometry and provides qualitative confirmation of the quantitative hydrogen retention measurements. Importantly, these visual observations reinforce the conclusion that the AMM end-cap coatings are critical in dictating the hydrogen preservation, as insufficient barrier performance results in marked dehydrogenation detectable both by weight-loss analysis and optical appearance of the recovered pellets.

4.3. Performance of AMM modules with multilayer (Two Al_2O_3 coupled with two Cr layers, net thickness ~1.2 µm) coated Nb end caps under Argon and Vacuum environments.

The AMM containing a niobium liner with a ~1.2 µm hydrogen permeation barrier, composed of alternating Cr and Al_2O_3 layers (2× Cr and 2× Al_2O_3), see figure 16 and Figure 17, was subjected to a two-stage thermal exposure campaign in order to evaluate the performance of this multilayer coating design in protecting the critical end-cap regions. The first stage of testing was performed under flowing argon atmosphere (1 atm, 50 sccm flow) at 750 °C for 500 h at Argonne. The H/Y ratio measurements collected at 100 h intervals revealed only a modest decrease in hydrogen content, amounting to ~2% total loss after 500 h. In contrast, when this same AMM module was shipped to Los Alamos National Laboratory (LANL)and subjected to high vacuum (~5×10^{-6} mbar) at an elevated temperature of 800 °C for an additional 500 h, the hydrogen loss

behavior was significantly different, where a ~7% hydrogen loss was found, which is substantially greater than when it was tested in argon, see figure 18 (a, b).

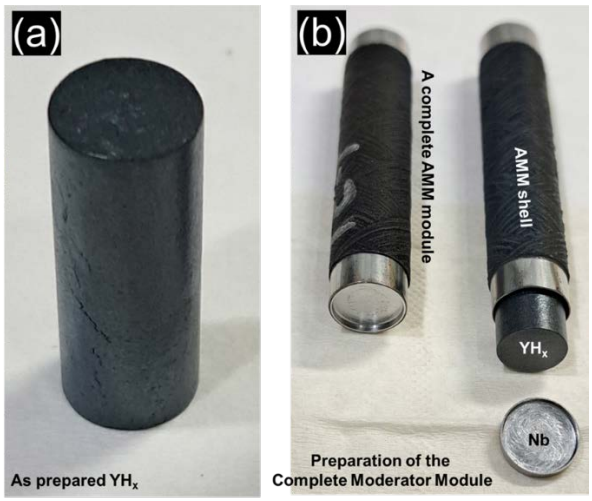

Figure 16. AMM module used for the two-step test with 1.2 µm ($2\times Al_2O_3 + 2\times Cr$) end-cap coating. (a) As-prepared YH_{2-x} pellet. (b) Coated AMM shell and a fully sealed module prior to testing.

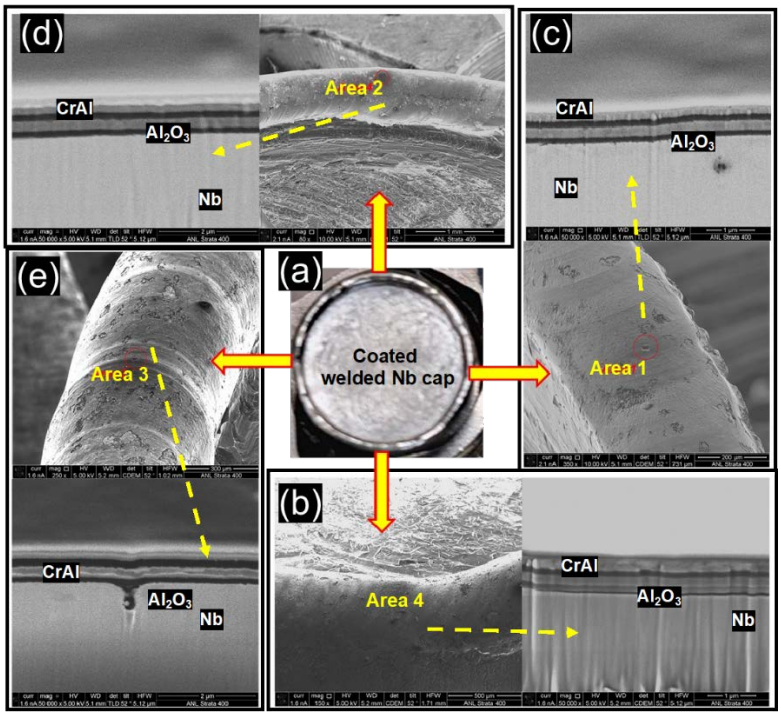

Figure 17: (a) Top view of the Nb end cap of an AMM, which was first welded to the AMM and then coated with the multilayer coating. (b, c, d, & e) showing a cross-sectional FIB-SEM view of the deposited multilayer coating, over the welded Nb cap surface. The FIB reveals a well-adhered uniform coating with no visible defects or separations in all four regions.

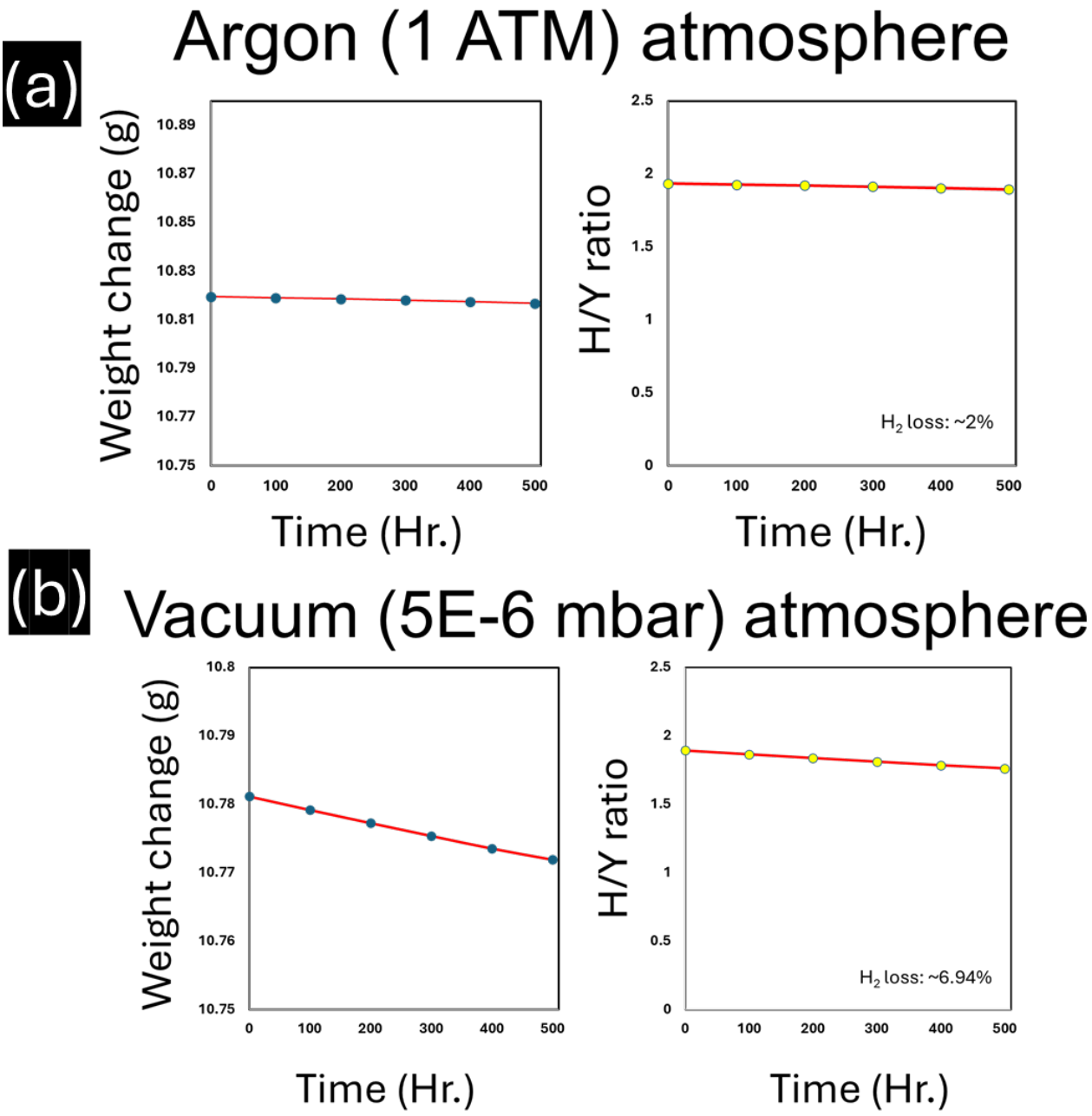

Figure 18. Hydrogen-loss trajectories for the same AMM module with the 1.2 µm multilayer on end caps, (a) Argon, 750 °C, 500 h at ANL: shallow, ~linear decline corresponding to **≈2 %** H loss. (b) High vacuum, 800 °C, 500 h at LANL: steeper decline corresponding to **≈7 %** H loss, attributed to tensile stress in vacuum plus Arrhenius increase in permeability and higher thermal-mismatch stresses at 800 °C.

Taken together, these findings emphasize the importance of both environmental conditions and coating thickness in ensuring long-term hydrogen retention. While the 1.2 µm Cr/Al_2O_3 multilayer performed adequately under argon by maintaining H_2 loss below ~2% after 500 h, its

performance degraded under vacuum at elevated temperature, resulting in a loss of ~7%. The results clearly demonstrate that the thinner multilayer structures are highly sensitive to both stress state and temperature, and while they may be viable in inert-gas–moderated applications, they are insufficient for vacuum-facing, high-temperature reactor conditions. This motivates the adoption of thicker multilayer designs (≥1.8–3.4 μm), which distribute stress more effectively, provide redundancy against local defects, and significantly reduce hydrogen permeation, thereby extending the durability and functionality of AMM modules under demanding service conditions, More details regarding the optimized design developed tested provided in the discussion section.

4.3.1. Post-Test Analysis of YH_{2-x} Pellet Appearance After Sequential Ar and Vacuum Exposures at Argonne and LANL.

Figure 19 (a) shows the as-prepared YH_{2-x} pellet with its characteristic uniform blue appearance, indicative of a near-stoichiometric YH_{2-x} phase with minimal surface degradation. After encapsulation within the AMM and exposure to 500 h at 750 °C in flowing argon at Argonne, followed by an additional 500 h at 800 °C under vacuum at LANL. The YH_{2-x} pellet (Figure b) used in this testing was recovered from the AMM, and it retained its overall structural integrity and exhibited a surface color that remained predominantly blue, but with localized regions of spotted discoloration.

This color evolution can be attributed primarily to progressive hydrogen depletion from the pellet surface during high-temperature exposure. In argon, the H_2 loss was relatively limited (~2% after 500 h), as the inert atmosphere suppressed the driving force for hydrogen escape, allowing the pellet to retain much of its original blue hue. However, under subsequent vacuum exposure at 800 °C, the hydrogen loss rate increased substantially (~7% after 500 h), driven by the large differential and higher temperature pressure. This accelerated depletion promotes the formation of slightly more yttrium-rich near-surface phases, which are known to exhibit metallic to darkened surface tones interspersed with residual blue coloration. The spotted discoloration observed is consistent with localized variations in hydrogen stoichiometry within the surface region, rather than bulk degradation.

Importantly, no evidence of oxidation or deleterious weight gain was detected during or after testing. The absence of surface oxides confirms that the AMM capsule retained hermeticity

throughout the exposure, with the only significant mass change attributable to controlled hydrogen out-diffusion. Thus, while the pellet shows visual signs of partial hydrogen loss, its phase purity and protective environment remain uncompromised.

Figure 19. Appearance of YH_{2-x} pellets before and after AMM exposure: (a) as-prepared pellet showing uniform blue coloration, and (b) pellet recovered after sequential thermal exposures (500 h in Ar at 750 °C at Argonne, followed by 500 h in vacuum at 800 °C at LANL), showing blue surface with localized spotted discoloration due to hydrogen depletion.

These results reinforce two critical findings: (i) hydrogen retention is strongly dependent on the external environment and driving pressure gradient, and (ii) the AMM design successfully

provides hermetic protection against oxidation, ensuring that long-term performance is limited only by permeation through the engineered caps rather than environmental ingress.

4.4. Analysis of the Performance of AMM modules with end caps coated 500 nm and 1.2 μm multilayer

4.4.1. Post-Test Examination of Single-Layer Al_2O_3 (500 nm) End-Cap Coated AMM.

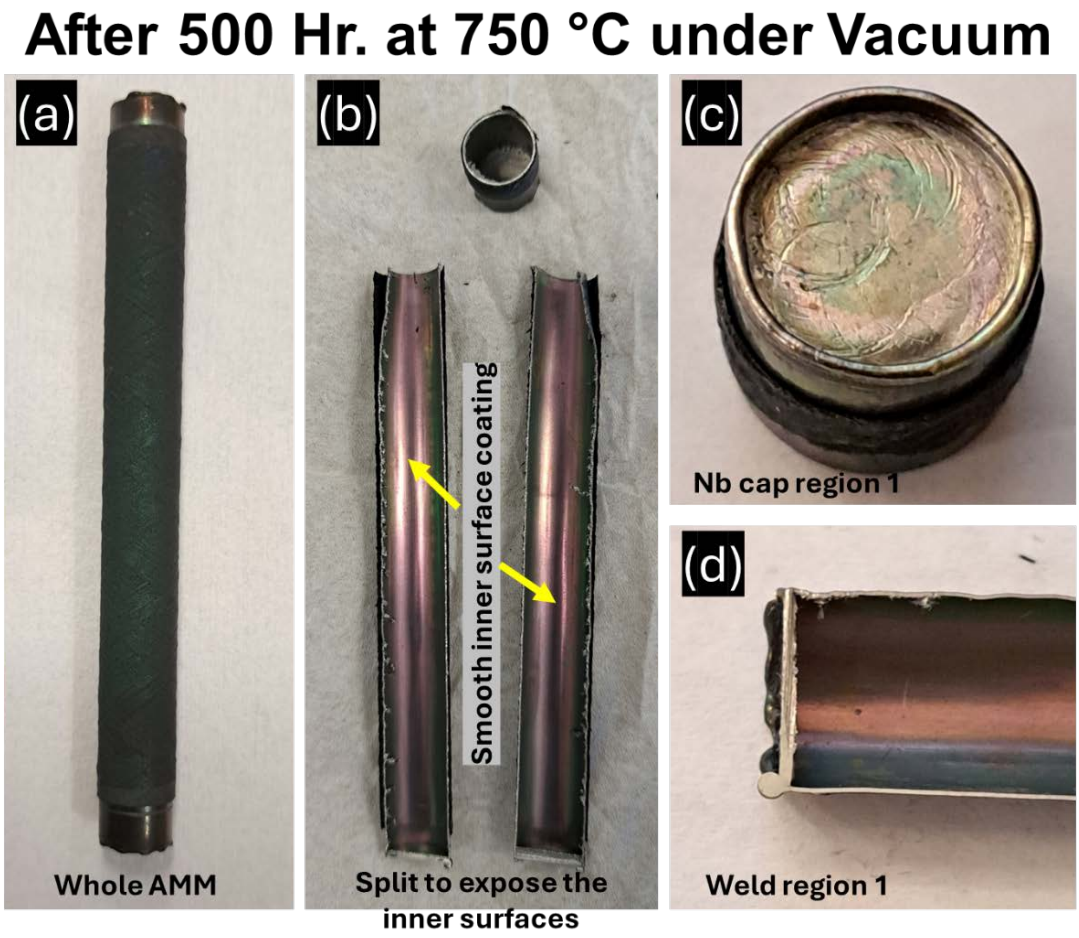

Figure 20. Post-test evaluation of AMM with single-layer Al_2O_3 (500 nm) cap coating after 500 h exposure under vacuum at 750 °C: (a) intact AMM, (b) sectioned view showing intact multilayer inner liner coating, (c) Nb cap region with localized discoloration, and (d) weld region showing no visible failure or coating degradation.

The AMM module employing a single 500 nm Al_2O_3 coating at the niobium (Nb) cap region was exposed to both argon and vacuum conditions for 500 h at 750 °C, after which the sample was sectioned and split open for detailed analysis. In this report, shown in Figure 20, we

are showing the AMM module that was under vacuum. The inner multilayer coating applied along the Nb liner remains smooth and intact after the exposure, with no observable signs of discoloration or spallation (Figure 20 b). This demonstrates that the optimized liner coating retained its barrier integrity and was resilient against hydrogen permeation and high-temperature vacuum exposure after 5 thermal cycling.

In contrast, localized surface discoloration was observed at the Nb cap region (Figure 20 c). Despite this slight discoloration, the weld inner edge regions (Figure 20 d) exhibited no obvious coating delamination or cracking, and the overall weld seam remained intact, suggesting the weld process did not compromise the hermetic sealing of the AMM. Importantly, no indications of oxygen ingress or mass gain were detected from the YH pellets that were collected from this module, confirming that the module remained hermetic during the test. The split surfaces were characterized under microscope to confirm the observations.

4.4.2. Microstructural Assessment of the Nb End Cap with Single-Layer Coating.

Detailed SEM analysis of the Nb end cap from the AMM module tested under vacuum at 750 °C for 500 h reveals clear evidence of localized coating failure in the form of **fractures and spallation** at the pan-shaped valley region (Figure 21 a–c). The optical overview (Figure 21 a) shows general discoloration across the Nb cap surface, while higher-magnification SEM images (Figures 21 b and c) highlight severe microstructural damage. Specifically, the single 500 nm Al_2O_3 coating exhibited **edge-localized cracking and delamination**, with fractures propagating radially across the coating and segments of the layer partially spalling off from the underlying Nb surface. Figure 21 (c’- c””) presents the EDS mapping results obtained from the fractured Nb cap region of the AMM module tested under vacuum at 750 °C for 500 h. These defects were further analyzed by EDS to determine the chemical composition across the cracked surfaces.

The combined layered EDS image (c′) shows distinct elemental distributions corresponding to aluminum (Al), oxygen (O), and niobium (Nb). The mapping highlights regions of disrupted coating coverage, particularly at the edges of fracture zones. The Al Kα1 map (c″) shows a continuous signal in regions where the Al_2O_3 coating is intact; however, areas adjacent to the cracks display discontinuities in Al distribution. Similarly, the O Kα1 map (c‴) mirrors the Al

distribution, confirming the presence of Al_2O_3 coating over much of the surface but also highlighting coating discontinuity near the fracture lines.

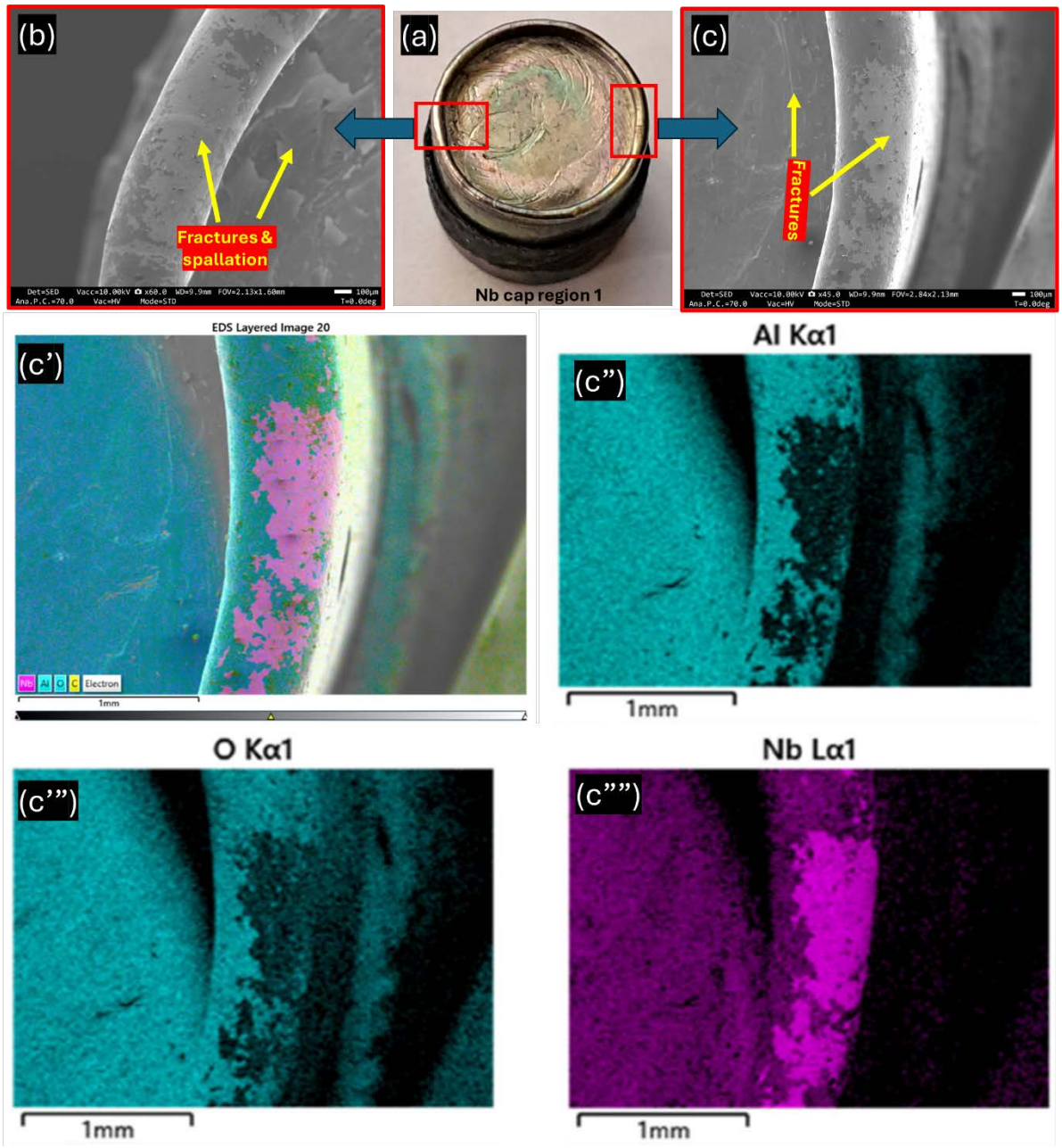

Figure 21. SEM & EDS evaluation of the Nb end cap from the AMM module tested under vacuum for 500 h. (a) Optical image of the Nb cap surface; (b, c) SEM micrographs of the pan-shaped valley regions, showing localized cracking and spallation of the 500 nm Al_2O_3 single-layer coating along the edge transition zones. (c′) layered EDS map showing combined Nb, Al, and O signals, (c″) Al Kα1 distribution, (c‴) O Kα1 distribution, and (c⁗) Nb Lα1 distribution. Clear Nb signal confirms coating loss and substrate exposure in fractured regions of the single-layer Al_2O_3 design.

The most significant result is observed in the Nb Lα1 map (c‴), which clearly reveals strong Nb signals in the fractured regions. This indicates direct exposure of the Nb substrate due to coating delamination and loss in those locations. The localized Nb visibility aligns with the SEM observations of crack propagation and spallation, providing direct chemical evidence that the single-layer 500 nm Al_2O_3 coating has failed to maintain complete surface coverage at the cap region.

4.4.3. Optical Examination of Recovered AMM with Multilayer (Two Al_2O_3 Layers and Two Cr Layers) Coated Nb Cap Region.

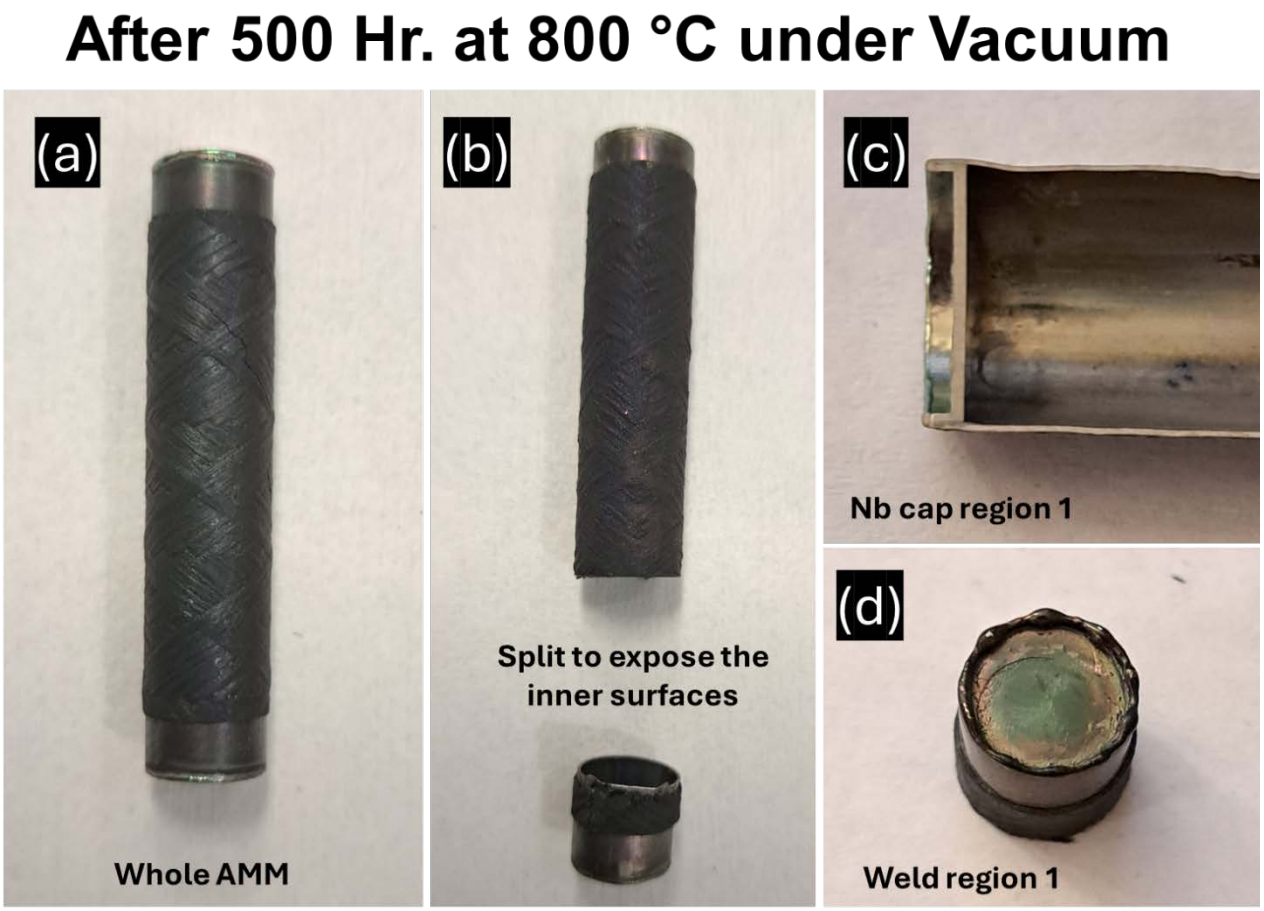

Figure 22. Optical images of the AMM module with multilayer-coated Nb cap region (2 × 300 nm Al_2O_3 + 2 × 300 nm Cr). (a) Whole AMM module following thermal testing, (b) split AMM exposing intact inner surfaces, (c) Nb cap region showing slight discoloration, and (d) weld region highlighting surface features following exposure.

The AMM module prepared with a multilayer cap coating architecture consisting of two 300 nm Al_2O_3 layers and two 300 nm Cr layers was subjected to 500 hours of thermal exposure under argon at ANL at 750 °C, followed by an additional 500 hours under vacuum at 800 °C at LANL. Following testing, the module was sectioned to allow direct optical examination of the interior surfaces, the Nb cap regions, and weld areas.

Figure 21 shows the post-test condition of the recovered AMM module. The whole module prior to sectioning (a) retains its structural integrity, with no visible surface deformation or macroscopic defects. Upon splitting the AMM to expose the internal surfaces (b), visually the multilayer inner coating is observed to remain intact, presenting a uniform appearance without any noticeable discoloration along the liner region. Examination of the Nb cap region (c) indicates the presence of slight discoloration localized on the cap surface, while the weld region (d) shows a distinct contrast in color and surface texture relative to the liner interior. Both weld and cap surfaces remain clearly visible and distinct under optical observation.

4.4.4. EDS Mapping of Nb End Cap Region with Two Al_2O_3 + Two Cr Layer Coating.

Figure 23 presents the EDS mapping and elemental distribution from the Nb end cap region coated with a multilayer architecture comprising two Al_2O_3 layers and two Cr layers. The optical image of the examined end cap (a) shows the overall condition of the coated region following testing, with visible surface texture and color variation across the cap face. The composite EDS layered map (b) provides a spatial distribution of elements over the examined area, combining signals from Nb, Al, Cr, and O.

The elemental distribution maps highlight the localized presence of each element: the Al $K\alpha_1$ map (c) shows the aluminum signal primarily concentrated near the cap surface regions, while the Cr $L\alpha_{1,2}$ map (d) exhibits chromium coverage across a broad portion of the analyzed surface. The Nb $L\alpha_1$ map (e) reveals clear regions of exposed niobium signal through the cap face, confirming that the substrate is directly detected in several zones of the examined region.

Together, the optical (a), composite EDS (b), and elemental maps (c–e) provide a direct view of the surface condition of the multilayer-coated Nb end cap, with Nb being prominently visible in the elemental map, and confirms the double layer design was also insufficient to take the stresses generated under vacuum at 800 °C.

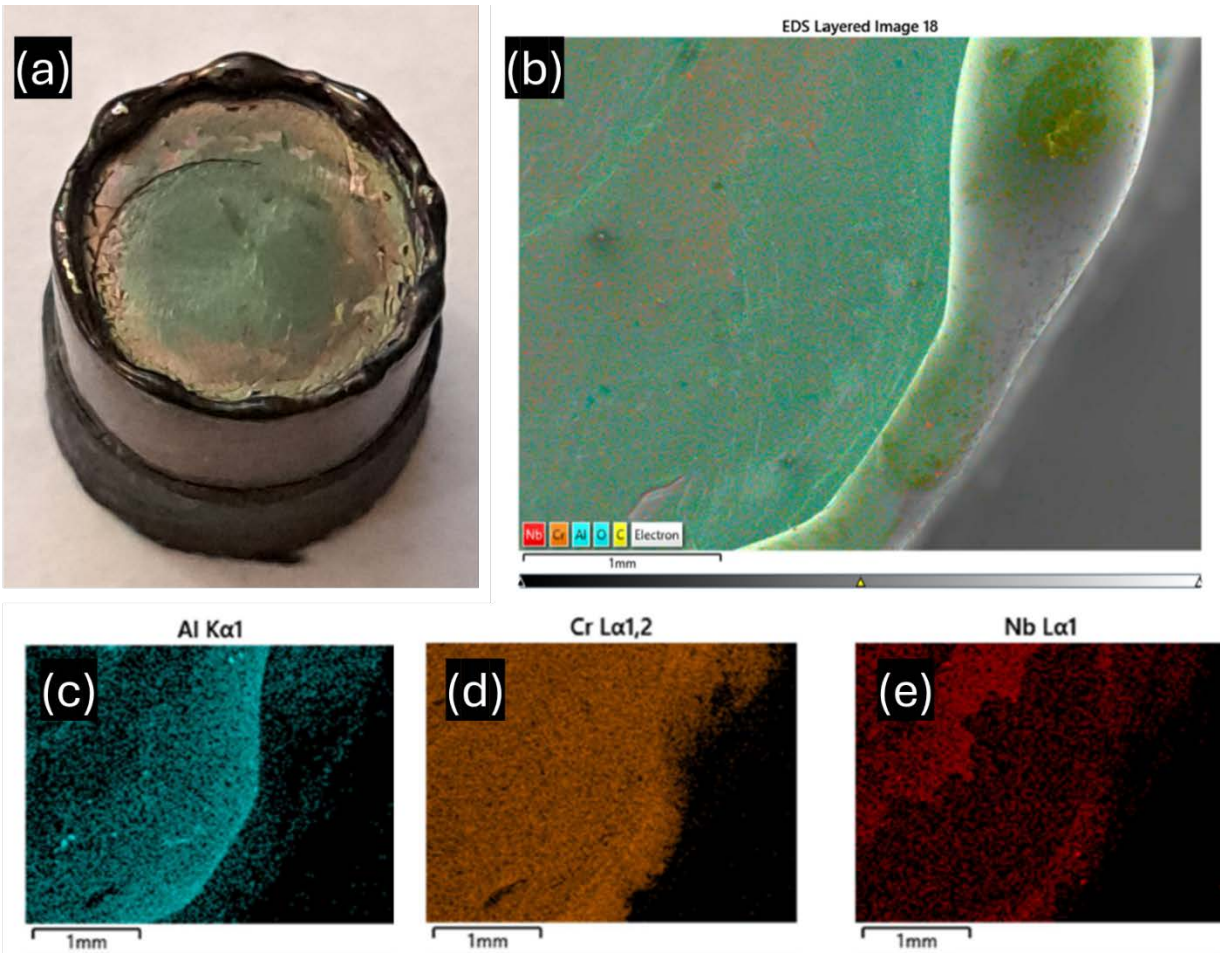

Figure 23. EDS mapping and elemental analysis of the Nb end cap region coated with two Al_2O_3 + two Cr layers. (a) Optical image of the coated end cap, (b) composite layered EDS map, (c) Al $K\alpha_1$ distribution, (d) Cr $L\alpha_{1,2}$ distribution, and (e) Nb $L\alpha_1$ distribution.

4.4.5. FIB Cross-Sectional Analysis of Optimized Multilayer Coating Present on the Outside and Inside Surfaces of the Cylindrical Nb Liner.

Figure 24 presents the focused ion beam (FIB) cross-sectional analysis of the optimized multilayer coating applied to the Nb liner surface of the AMM module, following extended thermal exposure at 800 °C under vacuum for 500 hours. The optical image of the intact AMM outer surface (a) and the corresponding cross-sectional micrograph (a′) clearly reveal the preservation of the periodic multilayer architecture. Distinct alternating Cr and Al_2O_3 layers remain continuous, with no evidence of large-scale cracking, delamination, or spallation.

Similarly, examination of the inner surface (b) and its high-magnification FIB section (b′) further confirms the structural stability of the multilayer design. The layer sequence is retained, with sharp interfaces visible between the ceramic and metallic layers, despite the severe thermo-mechanical stresses imposed by high-temperature vacuum exposure.

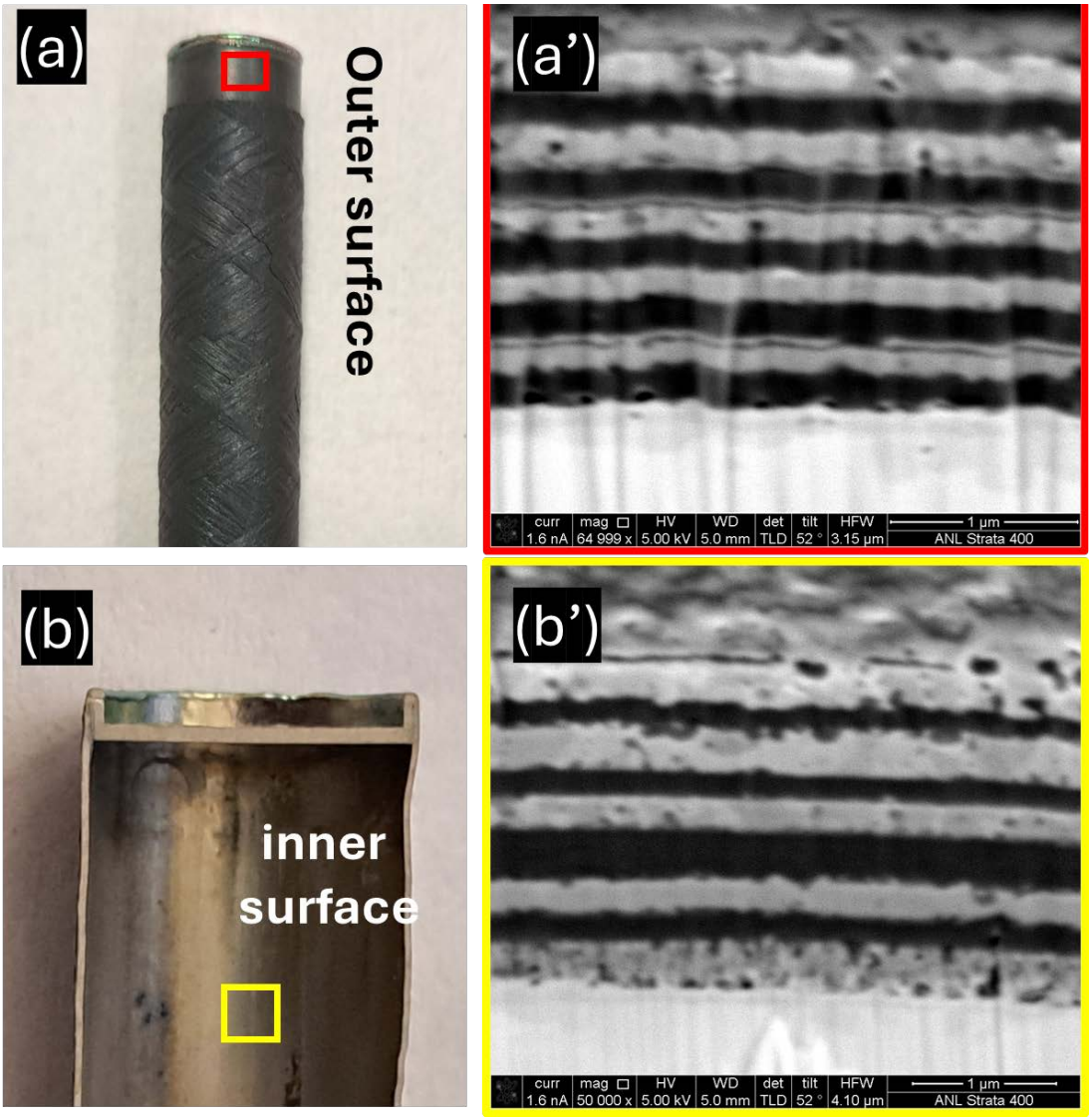

Figure 24. FIB cross-sectional analysis of the optimized multilayer coating on the Nb liner surface of the AMM module tested under vacuum at 800 °C for 500 h. (a) Optical image of the outer surface, (a′) FIB cross-section from the outer surface, (b) optical image of the inner surface, and (b′) FIB cross-section from the inner surface showing intact multilayer structure. The analysis confirms coating stability and indicates that hydrogen loss arises from Nb end-cap regions rather than the optimized multilayer-coated liner surface.

This observation contrasts sharply with the previously analyzed single-layer (500 nm Al_2O_3) and two-layer (Al_2O_3 + Cr) coatings at the end-cap regions, which displayed fracture, spallation, and local coating failure under similar or less aggressive conditions. In contrast, the optimized multilayer system shown here demonstrates excellent thermal and mechanical resilience, highlighting its ability to survive reactor-relevant environments.

Importantly, this FIB cross-sectional analysis also confirms that the hydrogen loss previously observed in the results section originates predominantly from the Nb end-cap regions, where simplified coating designs were prone to failure. The intact multilayer coating over the Nb liner surface itself shows no signs of degradation, indicating that the optimized multilayer architecture remains highly effective at impeding hydrogen permeation.

4.4.6. Weld Integrity Analysis of AMM Nb Cap Regions under Thermal Cycling.

The weld regions of the AMM niobium (Nb) caps were examined to evaluate their structural integrity after extended high-temperature testing, including multiple thermal cycling experiments. Figures 25 (a) and (b) present the optical micrographs of the weld regions for both the single-layer coated Nb cap AMM and the multilayer-coated Nb cap AMM, respectively. To further probe these regions, high-resolution scanning electron microscopy (SEM) was conducted at the highlighted locations, corresponding to regions 1–4 as indicated in the optical images.

The SEM micrographs of regions 1 and 2 (Figures 25 a′ and a″) and regions 3 and 4 (Figures b′ and b″) clearly demonstrate that the weld seams remain continuous and defect-free, without signs of cracking, or void formation, even after prolonged exposure to high temperatures and repeated thermal cycling. The fusion zone and the heat-affected zone (HAZ) appear structurally sound, with no evidence of porosity or degradation that might otherwise compromise hermeticity.

This analysis confirms that the welds have retained their mechanical and hermetic integrity throughout the testing period. Therefore, the welds themselves did not contribute to the excess hydrogen loss observed in certain AMM configurations. The hydrogen permeation behavior is thus attributable to the coating performance on the Nb cap regions rather than any weld-related leakage pathway.

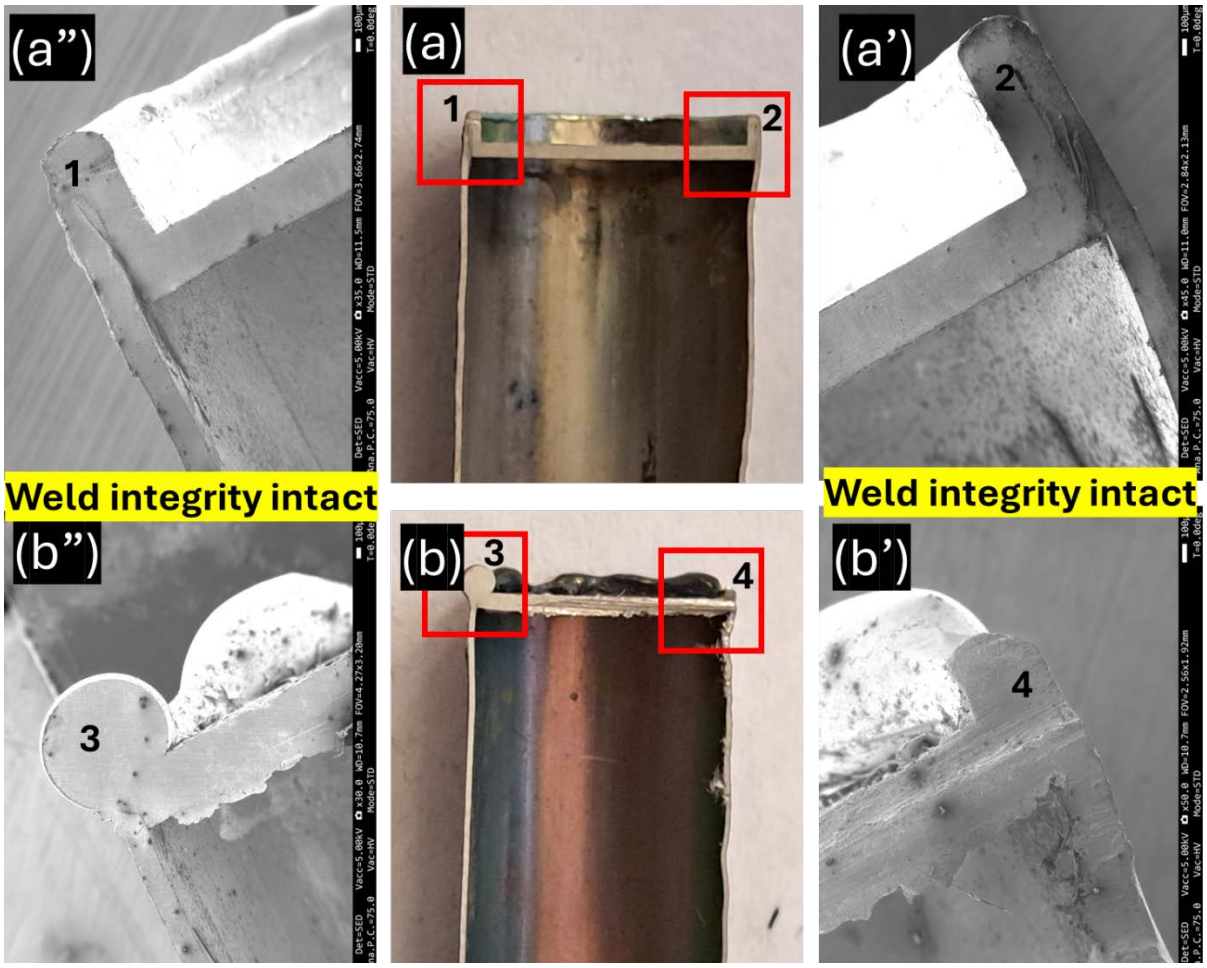

Figure 25. Optical micrographs of AMM Nb weld cap regions for single-layer (a) and multilayer (b) coated designs, alongside corresponding SEM images from regions 1–4 (a′, a″, b′, b″). All examined regions confirm weld integrity remains intact even after extended high-temperature cycling.

4.4.7. Hoop Stress Distribution in 500 nm Al_2O_3 Single-Layer Cap Coating and Its Role in Failure.

The hoop stress analysis presented in the figure 26 (b) highlights the mechanical limitations of the 500 nm Al_2O_3 single-layer coating applied to the Nb cap region at 750 °C. Under vacuum conditions (orange curve), the coating experiences outward-driven tensile stress that decreases from ~250 MPa near the inner radius to ~185 MPa at the rim. Conversely, under argon (blue curve), the coating is subjected to inward compressive stress that progressively increases from ~200 MPa at the center to ~271 MPa at the rim. Importantly, both stress states intersect the

thermally induced baseline (~225 MPa), but near the rim, the stresses fall within the failure-prone region (highlighted in red).

The single thin Al_2O_3 coating lacks sufficient thickness and structural redundancy to distribute or absorb these rim-concentrated stresses. As a result, the material undergoes localized cracking and spallation near the edge, where stress intensification is greatest. This explains the experimentally observed fractures in the single-layer caps under both vacuum and argon atmospheres. The analysis demonstrates that the failure mechanism is dominated by stress concentration at the rim combined with the inherently brittle nature of thin Al_2O_3 films, making them particularly vulnerable compared to multilayer architectures.

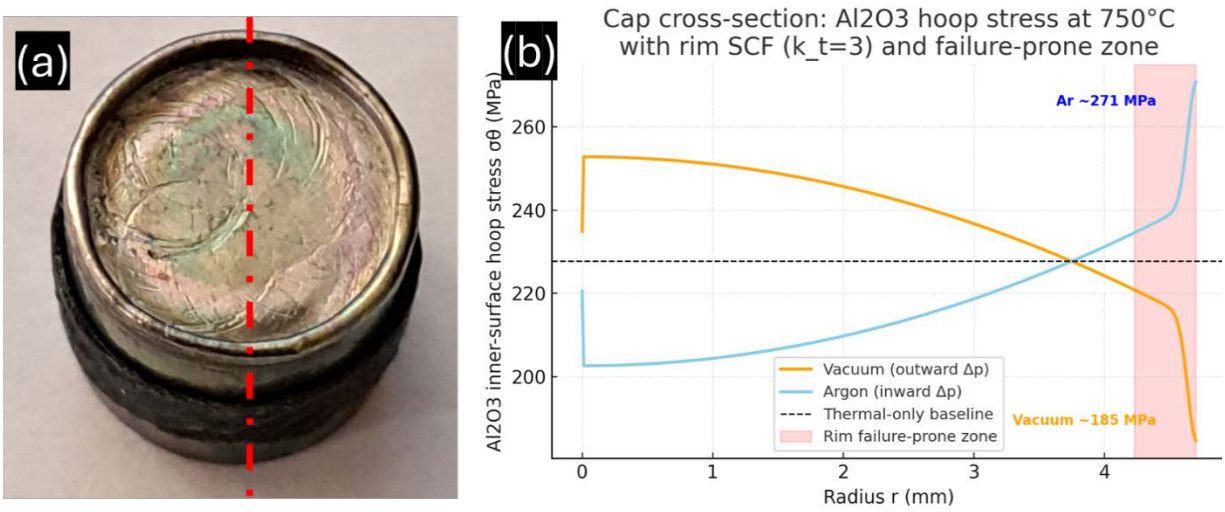

Figure 26. Hoop stress distribution in a 500 nm Al_2O_3 single-layer coating at 750 °C under vacuum and argon environments, showing rim stress concentrations driving fracture and coating failure.

4.4.8. Hoop Stress Distribution and probable Failure cause for 1.2 µm Multilayer (2×Cr + 2×Al_2O_3) Coatings on Nb End Caps especially under vacuum.

Figure 27 presents the combined experimental and modeling analysis of the Nb end cap coated with the 1.2 µm multilayer stack (2×Cr-300 nm + 2×Al_2O_3-300 nm). Panel (a) shows the recovered end cap after testing under vacuum at 800 °C, revealing visible surface discoloration and partial degradation at the cap edges. The inset cross-sectional SEM confirms the multilayer coating architecture, consisting of alternating Cr and Al_2O_3 layers deposited on the Nb substrate. Panel (b) plots the modeled hoop stress distribution across the cap cross-section at 750 °C under both

vacuum (outward Δp) and argon (inward Δp) conditions. While the stress at the central region remains modest (≈18–20 MPa), the stress rises sharply toward the rim, exceeding ≈50 MPa in both environments. The shaded red band highlights this rim zone, which represents the most failure-prone region due to geometric stress concentration and mismatch-driven strain localization. The correlation between the elevated hoop stress at the rim and the observed discoloration/failure in panel (a) provides clear evidence that coating breakdown initiates at these localized high-stress regions, even though the central multilayer film retains structural integrity .

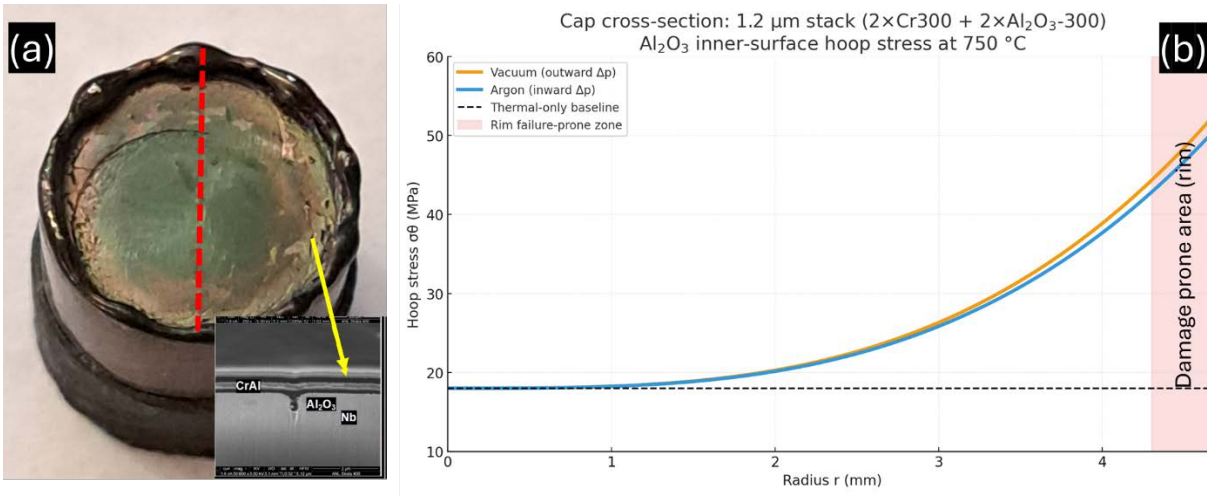

Figure 27. Hoop stress distribution in the Nb end-cap region coated with a 1.2 μm multilayer stack (2×Cr-300 nm + 2×Al_2O_3-300 nm) tested at 750 °C, showing stress concentration at the rim and correlation with observed coating failure.

Incidentally, under Argon atmosphere, the thin multilayer coating (2×Al_2O_3-300/2×Cr-300, ≈1.2 μm) exhibited only ~2% hydrogen loss, while under vacuum it lost ~7%, reflecting the very different mechanical and transport conditions at the cap rim. In the argon environment, the external pressure creates a small inward Δp that adds compressive hoop stress to the thermal-mismatch baseline, suppressing crack opening, reducing the effective stress intensity at flaws, and thereby maintaining hermeticity. This effect is reinforced by the inert gas atmosphere, which lowers the net hydrogen chemical-potential gradient across the coating and limits permeation driving force. In contrast, in high vacuum (~5×10^{-6} mbar), the Δp reverses to outward, producing tensile hoop stresses that promote crack opening and interfacial peeling in the rim stress-concentration zone. Once microcracks form, the nearly zero external P_{H2} maximizes the driving

force for hydrogen effusion, sharply increasing flux through defects. Moreover, the vacuum tests were performed at 800 °C, higher than the 750 °C argon runs, further elevating diffusion and thermal mismatch strains. Together, these factors explain why the thinner multilayer survives relatively well under argon but fails under vacuum, highlighting the importance of compressive stress states and reduced chemical gradients for retaining hydrogen in brittle ceramic coatings.

Consequently, the thinner coatings (0.5–1.2 μm) repeatedly show fracture and spallation at the Nb cap regions under thermal cycling and vacuum exposure, it is scientifically justified to move toward a thicker multilayer design. A thicker multilayer is expected to distribute the thermal mismatch strain more evenly across multiple plies, introduce additional crack-arresting interfaces, and provide redundancy in hermetic sealing. These combined factors should enhance the coating's tolerance to localized rim stresses and prevent the through-cracks that compromise hydrogen retention in the thinner architectures.

4.5. Performance of AMM modules, without SiC composite shell, with thicker multilayers (Four Al_2O_3 coupled with four Cr layers, net thickness ~3.2 μm) coated Nb end caps under Argon and Vacuum environments.

AMM modules were fabricated **without** the external SiC composite shell and with 3.2 μm thick multilayers (4×Al_2O_3–300 nm / 4×Cr–500 nm) deposited over the Nb cap regions. Testing of those modules avoids the complications of degassing of the SiC composite and its interference with the measurement of hydrogen losses, as well as validate the robustness of the optimized multilayer coating design with thicker overall architecture. Those modules were tested, directly probing the coating's standalone mechanical and hermetic stability. The modules were evaluated under two environments: (i) argon atmosphere (1 atm) at 750 °C for 300 hours, with weight data recorded every 100 hours, and (ii) vacuum (~5×10^{-6} mbar) at 750 °C for 300 hours, with weight data collected at the same intervals.

As shown in Figure 28, the optical appearance of both post-test AMM modules remained unchanged, with no signs of cap deformation or surface spallation under either environment. Importantly, the Nb cap regions coated with the multilayer stack showed no evidence of cracking or discoloration, confirming that the thicker multilayer architecture remains adherent and mechanically resilient even at these elevated temperatures. Figure 29 further quantifies the

hydrogen retention behavior: in argon (a), the hydrogen mass remained essentially constant throughout the 300-hour test, while in vacuum (b), the behavior was similarly stable, with no significant hydrogen loss observed.

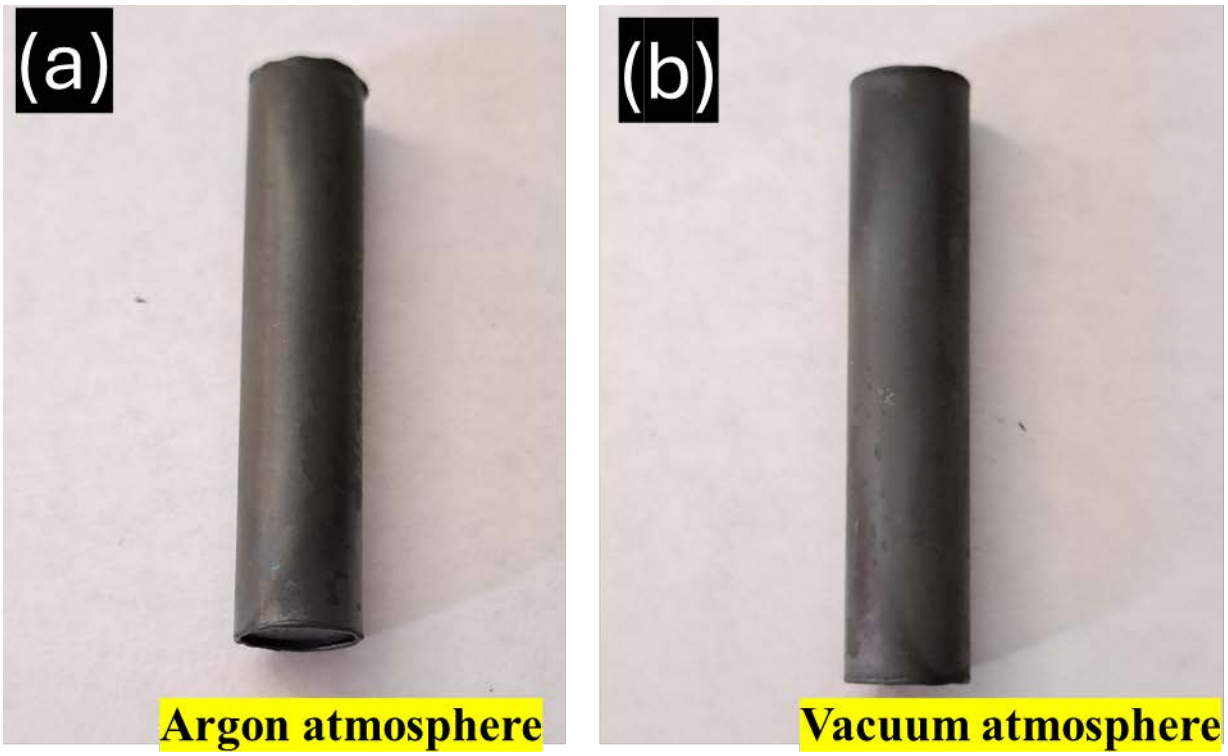

Figure 28. Optical images of recovered AMM modules with 3.2 μm multilayer coatings tested at 750 °C for 300 hours: (a) under argon atmosphere, and (b) under vacuum. Both show stable surfaces without spallation or visible degradation, particularly at the Nb cap regions, confirming structural integrity without SiC shell support.

These results demonstrate that the thicker multilayer coating provides effective resistance to crack opening, spallation, and hydrogen permeation at the Nb cap regions under both compressive (argon) and tensile (vacuum) stress biases, even in the absence of SiC shell mechanical reinforcement. This outcome confirms that at 750–800 °C the multilayer itself provides a sufficient hermetic barrier for hydrogen retention over extended durations.

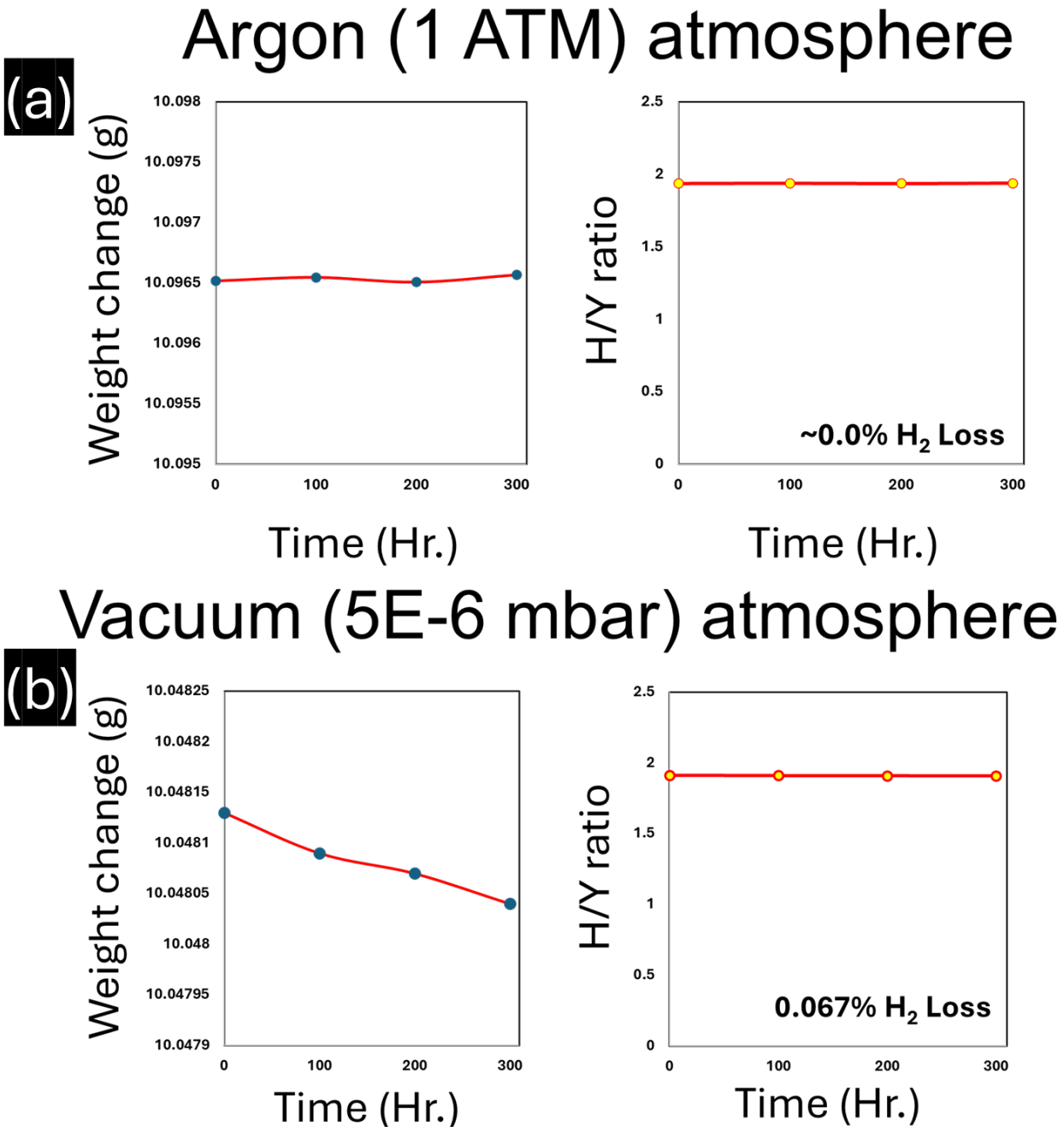

Figure 29. Measured hydrogen weight retention profiles for the 3.2 µm multilayer-coated AMM modules tested at 750 °C: (a) under argon atmosphere for 300 hours, and (b) under vacuum for 300 hours. Both conditions show negligible hydrogen loss, indicating excellent hermetic performance of the multilayer stack at the Nb cap regions.

4.5.1. Validation of Stress Dissipation through Multilayer Coating at Weld Edges.

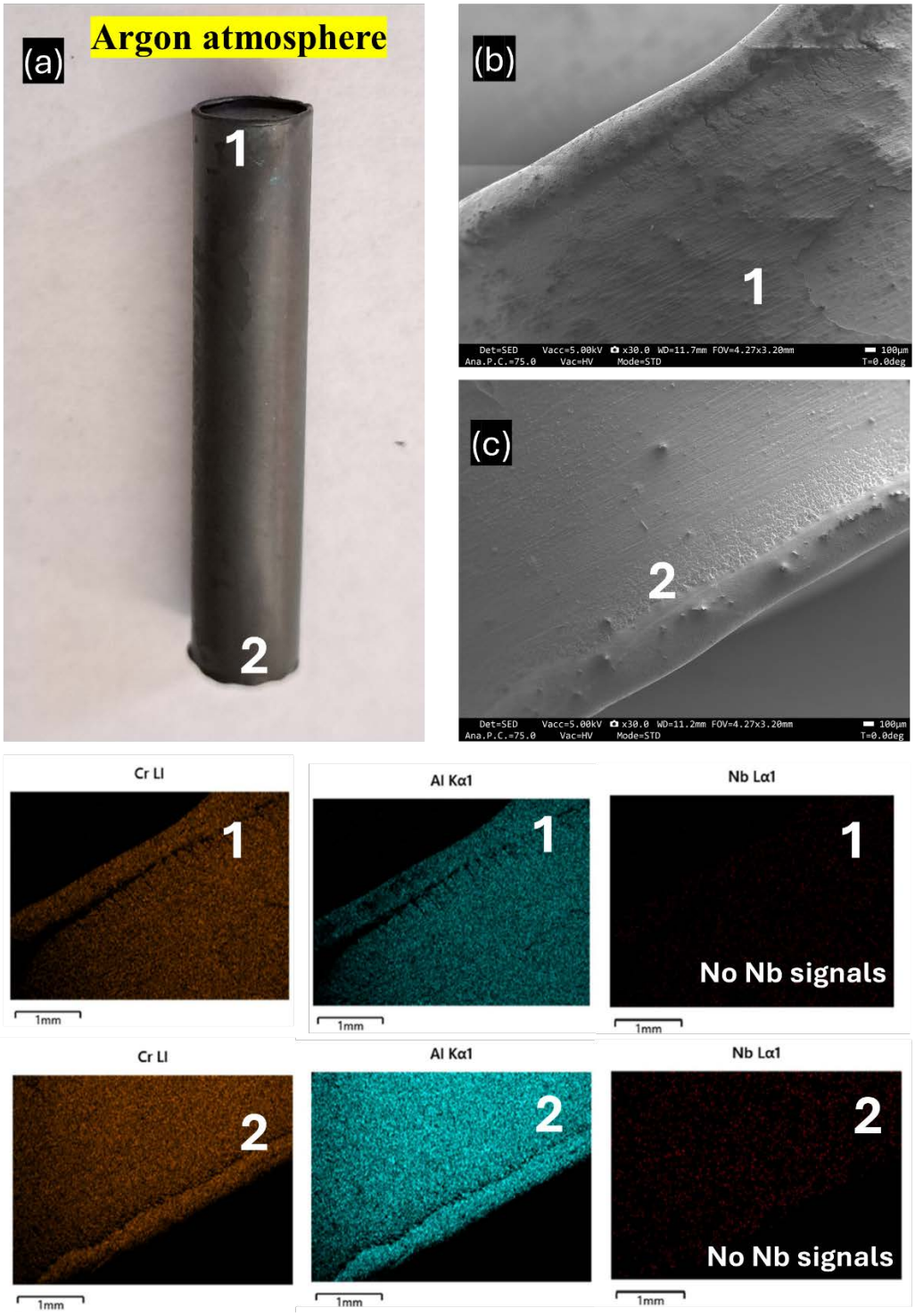

Figure 30. SEM–EDS analysis of the **Nb cap weld edges with a 3.2 μm thick multilayer coating, from the AMM tested under argon atmosphere** showing intact multilayer coating with no cracks, spallation, or Nb exposure.

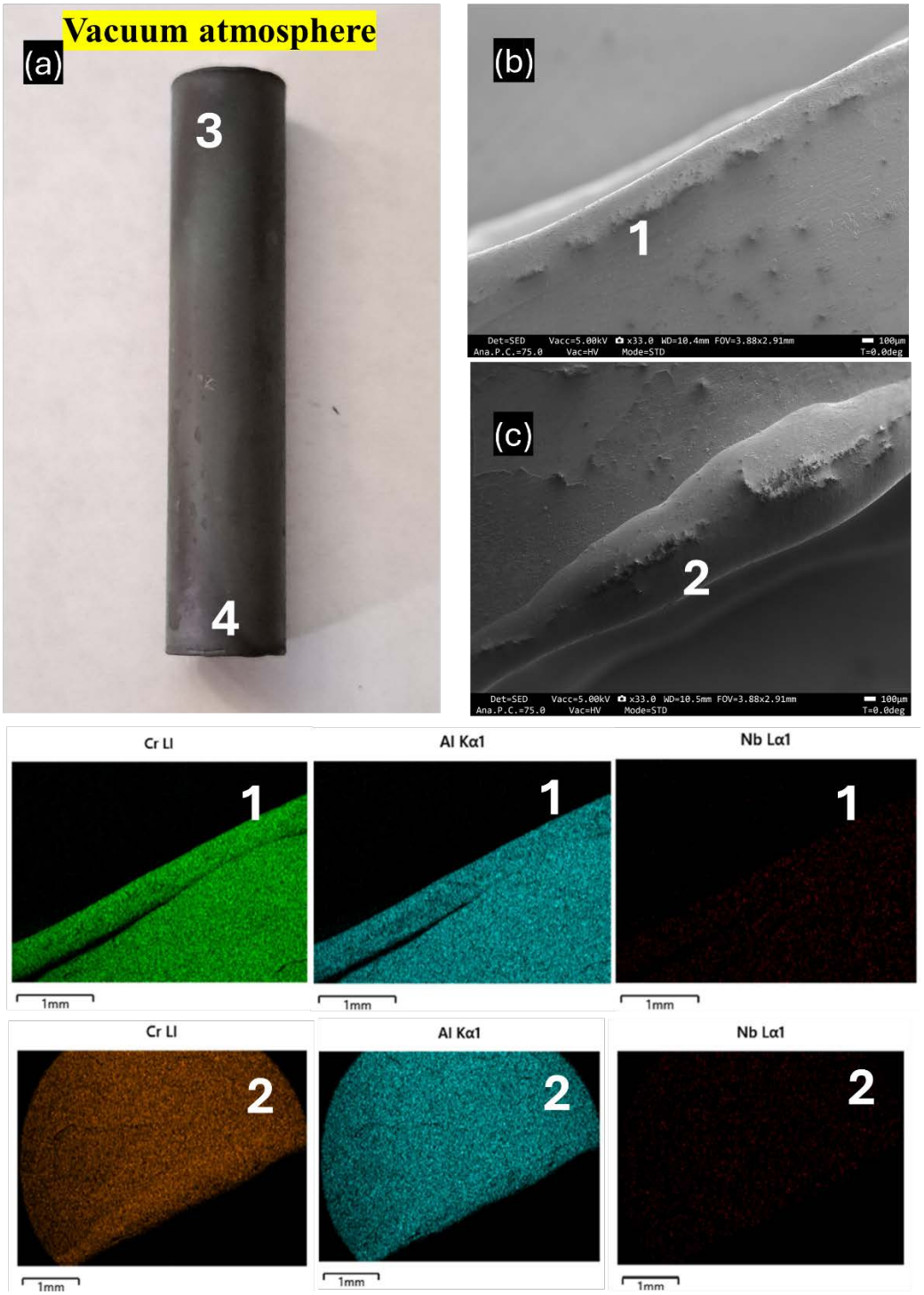

Figure 31. SEM–EDS analysis of the **Nb cap weld edges from the AMM with 3.2 μm coated end cap, tested under vacuum atmosphere** demonstrating continuous multilayer coverage and absence of Nb signals, validating the stress-relief effect of multilayer stacking.

The SEM–EDS analysis of the AMM modules tested under both argon (Figure 30) and vacuum (Figure 31) atmospheres demonstrates that the thicker multilayer design (~3.2 µm, comprising alternating Cr and Al_2O_3 layers) effectively suppresses coating degradation at the weld edges. In both cases, the microstructural examination did not reveal any signs of cracking, delamination, or spallation at the highly stress-concentrated rim and weld regions, locations where failure was observed in thinner single- and double-layer coatings. The absence of Nb signals in the EDS maps further confirms that the coating remains continuous and hermetic, with no exposure of the underlying substrate. This validates the theoretical expectation that increasing the number of multilayers provides improved stress distribution, as the ductile Cr interlayers act as strain absorbers and reduce the driving force for crack initiation and propagation in the brittle Al_2O_3 plies. The results therefore indicate that the multilayer design not only improves mechanical resilience but also maintains integrity of the hydrogen barrier function across extended exposures in both inert and vacuum environments.

4.5.2 Hoop Stress Distribution for 3.2 µm Multilayer (4×Cr + 4×Al_2O_3) Coatings on Nb End Caps especially under Argonne and Vacuum environment.

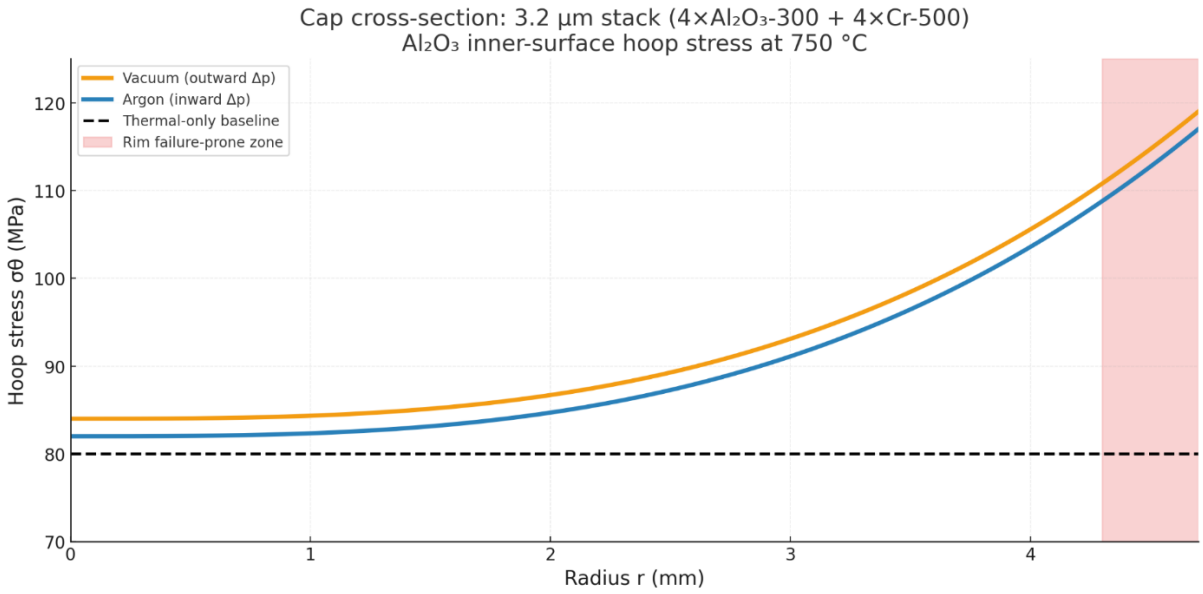

Figure 32: Hoop stress distribution in a 500 nm Al_2O_3 single-layer coating at 750 °C under vacuum and argon environments, showing rim stress concentrations driving fracture and coating failure.

The hoop stress analysis for the 3.2 μm multilayer stack (4×Al_2O_3–300 nm + 4×Cr–500 nm) shows tensile stresses ranging from ~80 MPa at the center to ~120 MPa near the rim, with vacuum producing slightly higher values than argon. Despite these higher absolute stresses compared to thinner multilayers, the stress is distributed more uniformly, reducing the effective driving force at flaw sites. This is consistent with SEM–EDS results, which revealed no cracks, spallation, or Nb exposure at the weld and rim regions after extended testing under both argon and vacuum. The elemental maps confirm intact Al_2O_3/Cr multilayers with no Nb signals, validating that the thicker architecture maintains hermeticity. These findings demonstrate that the 3.2 μm multilayer design can withstand elevated hoop stresses through mechanisms such as plastic relaxation in Cr layers, crack deflection at interfaces, and redundancy of multiple barriers, making it more resilient than thinner single- or double-layer coatings.

5. Conclusions

This study has demonstrated the successful fabrication, testing, and evaluation of Argonne's first Advanced Moderator Module (AMM) prototypes incorporating YH_{2-x} pellets, Nb liners, optimized multilayer coatings, and SiC CMC shells. The results highlight that while the Nb liner coatings provide a consistent and effective hydrogen permeation barrier, care must be taken in interpreting the hydrogen loss results during testing, due to the contributions from degassing from the SiC CMC shells. But another outcome of this study is the importance of the performance of the end-cap regions where care should be taken in providing additional layers of coating to further reduce hydrogen permeation.

Systematic testing of different end-cap coating architectures revealed that single-layer Al_2O_3 (0.5 μm) coatings are insufficient, permitting large hydrogen losses (>18–21%) under both argon and vacuum conditions. Intermediate multilayer coatings (≈1.2 μm, 2×Al_2O_3/2×Cr) improved retention under argon (~2% loss over 500 h) but degraded significantly in vacuum at elevated temperature (~7% loss at 800 °C). In contrast, thicker multilayer architectures (≈3.2–3.4 μm, 4×Al_2O_3/4×Cr to 8-layer stacks) demonstrated excellent performance, with negligible hydrogen loss under both argon and vacuum at 750 °C. These findings confirm that multilayer architecture and thickness are decisive in balancing permeation resistance, stress accommodation, and long-term durability.

Thermal-mechanical modeling and experimental analyses further helped to establish that environmental conditions play a dominant role: argon environments stabilize coatings through compressive bias, while vacuum environments impose tensile stresses and maximize chemical potential gradients, thereby accelerating failure in thinner coatings. Microstructural examinations (SEM/EDS, FIB) validated these interpretations. Importantly, weld integrity was maintained across all modules, confirming that hydrogen loss arises primarily from coating performance, not welding defects.

Taken together, the results establish that optimized multilayer end-cap coatings are essential for reliable AMM operation. By dissipating stress concentrations, introducing crack-arrest interfaces, and providing redundant permeation barriers, the multilayer approach enables simplified post-weld recoating strategies that ensure hermeticity while reducing fabrication complexity and cost. With demonstrated stability at 750–800 °C for extended exposures, the optimized AMM design is now poised for further in-reactor testing and integration into microreactor systems.

6. Future work

Building on the encouraging results from this study, several critical steps are planned to further validate and advance the Advanced Moderator Module (AMM) technology in FY 26:

1. **Extended Thermal Testing:**

   Long-term durability studies will be conducted at both ANL and LANL, using the latest modules designed with thicker end cap coatings, to extended exposure times ~1500–2000 hours at 750–800 °C under both argon and vacuum environments. These tests are essential to establish the long-duration stability of the optimized multilayer coatings and to assess their ability to maintain hermeticity under continuous operation.

2. **Alternate AMM Liner Materials:**

   While our current approach is focused on enhancing AMMs for high-temperature applications (up to 800 °C), some of the stakeholders are interested in lower temperature

applications, e.g. 650-700 ºC, which **will allow for simplification of the AMM containment design and fabrication** providing more **cost-effective design**. In this case, SiC composite/Nb liner can be replaced with common materials such as stainless steel or FeCrAl. Coating and testing of simplified designs will be performed.

3. **Neutron Irradiation Performance Evaluation:** Characterize an AMM enclosure irradiated at MIT during FY25, assessing the integrity of the barrier coatings, Nb liner, SiC structural enclosure, and welds. This irradiated sample will provide valuable insights into the long-term in-reactor performance of the full AMM assembly and identify critical degradation modes contributing to hydrogen loss.

7. References

[1] DOE Microreactor Program, Gateway for Accelerated Innovation in Nuclear (n.d.). https://gain.inl.gov/doe-microreactor-program/ (accessed August 29, 2024).

[2] DOD Exercises Option on Second Micro Nuclear Reactor Design, U.S. Department of Defense (n.d.). https://www.defense.gov/News/Releases/Release/Article/3524458/dod-exercises-option-on-second-micro-nuclear-reactor-design/https%3A%2F%2Fwww.defense.gov%2FNews%2FReleases%2FRelease%2FArticle%2F3524458%2Fdod-exercises-option-on-second-micro-nuclear-reactor-design%2F (accessed August 29, 2024).

[3] M.G. McKellar, D.P. Guillen, Effect of climate and component performance on optimized recuperated air Brayton cycles for nuclear microreactor power conversion, Progress in Nuclear Energy 162 (2023) 104761. https://doi.org/10.1016/j.pnucene.2023.104761.

[4] B. Cheng, E.M. Duchnowski, D.J. Sprouster, L.L. Snead, N.R. Brown, J.R. Trelewicz, Ceramic composite moderators as replacements for graphite in high temperature microreactors, Journal of Nuclear Materials 563 (2022) 153591. https://doi.org/10.1016/j.jnucmat.2022.153591.

[5] Y. Miao, N. Stauff, S. Bhattacharya, A. Yacout, T.K. Kim, Advanced Moderation Module for High-Temperature Micro-Reactor Applications, Argonne National Lab. (ANL), Argonne, IL (United States), 2020. https://doi.org/10.2172/1656612.

[6] Full article: Considerations for Hydride Moderator Readiness in Microreactors, (n.d.). https://www.tandfonline.com/doi/full/10.1080/00295450.2022.2121583 (accessed August 29, 2024).

[7] S. Bhattacharya, Y. Miao, A.M. Yacout, Development of Hydrogen Permeation Barrier and Matrix Interaction Protection Coatings for TZM Enclosure of Hydride Moderators (Microreactor Program M3 Report), Argonne National Laboratory (ANL), Argonne, IL (United States), 2023. https://doi.org/10.2172/1984639.

[8] S.G. Lee, J. Fourcade, R. Latta, A.A. Solomon, Polymer impregnation and pyrolysis process development for improving thermal conductivity of SiCp/SiC–PIP matrix fabrication, Fusion Engineering and Design 83 (2008) 713–719. https://doi.org/10.1016/j.fusengdes.2008.04.008.
[9] Gas tungsten arc welding, Wikipedia (2024). https://en.wikipedia.org/w/index.php?title=Gas_tungsten_arc_welding&oldid=1228153933 (accessed August 29, 2024).

Chemical & Fuel Cycle Technologies Division
Argonne National Laboratory
9700 South Cass Avenue, Bldg. 205
Argonne, IL 60439

www.anl.gov